DOI: 10.4408/IJEGE.2017-01.O-03

# MODELING OF RAPID FINE-GRAINED MATERIAL FLOWS

Francesco FEDERICO & Chiara CESALI

*University of Rome Tor Vergata - Department of Civil and Information Engineering - Rome, Italy*
*Corresponding author: fdrfnc@gmail.com*

## EXTENDED ABSTRACT

La previsione dei movimenti di versante e la progettazione di adeguate misure di mitigazione e protezione richiedono una profonda conoscenza dei processi fisici e meccanici che ne governano la propagazione. Tale conoscenza non può che derivare dall'esperienza, opportunamente interpretata e verificata mediante specifici modelli reologici.

Con il termine di movimenti di versante si indica la mobilitazione e lo scorrimento lungo versanti di masse fluide e/o granulari per effetto della forza di gravità.

Tali fenomeni (e.g. *normal stream flows, hyperconcetrated flows, mudflows, debris flows, rock avalanches*) sono caratterizzati da specifici comportamenti meccanici, dipendenti dalla loro natura plurifase (*flow like* e/o granulare) e dalle proprietà fisiche (e.g. granulometria, concentrazione volumetrica).

Nel presente articolo sono esaminati in dettaglio i flussi rapidi di materiale a grana fine (*fine-grained material flows, rapid mudflows*), caratterizzati generalmente da elevate concentrazioni di limo e argilla, notevole distanza percorsa, elevate velocità, fino a 25-30 m/s (e.g. le colate di fango che hanno devastato Sarno e Quindici nel 1998).

Diversi sono i fattori di innesco: intense precipitazioni, terremoti, escursioni termiche, attività dell'uomo.

I meccanismi di innesco e successiva propagazione di un flusso di materiali a grana fine dipendono principalmente dalla generazione, e possibile dissipazione (durante il moto, a causa di processi di consolidazione) di sovrappressioni interstiziali.

La considerevole riduzione della resistenza al taglio dovuta alla presenza di sovrappressioni interstiziali determina una elevata mobilità dei flussi di materiali a grana fine, anche lungo versanti di debole pendenza; inoltre, elevate pressioni interstiziali possono indurre la parziale o completa liquefazione del materiale. Al contrario, il processo di consolidazione durante il moto può progressivamente ridurre le pressioni interstiziali e il corrispondente incremento della resistenza al taglio limita la propagazione della massa in rapido scorrimento. In generale, la cinematica di un flusso granulare può essere inoltre notevolmente influenzata dalla variazione di massa dovuta ai processi di erosione del fondo e/o delle sponde dei canali lungo i quali avviene il moto.

Per stimare le variabili cinematiche (e.g. massima distanza percorsa e velocità raggiunta) di un flusso di materiali a grana fine, è stato elaborato un modello analitico dello scorrimento di un blocco. Sono prese in considerazione (i) la geometria (curvatura) della superficie di scorrimento; (ii) la possibile variazione di massa dovuta ai processi di erosione; (iii) le pressioni interstiziali alla base della massa in movimento e, in particolare, l'evoluzione delle sovrappressioni interstiziali (generazione iniziale dovuta a differenti fenomeni quali terremoti e, durante il moto, alla curvatura della superficie di scorrimento e alle condizioni non drenate ed edometriche del materiale; dissipazione dovuta al processo di consolidazione).

L'equazione differenziale che descrive lo scorrimento del blocco è stata integrata numericamente. Sotto alcune ipotesi semplificative è possibile risolverla anche in forma chiusa, recuperando due soluzioni note, come casi limite.

Sono state effettuate alcune analisi parametriche al fine di valutare il ruolo dei fattori introdotti (i.e. variazione della massa, curvatura della superficie di scorrimento, evoluzione delle pressioni interstiziali).

Gli aspetti legati alla possibile generazione di sovrappressioni interstiziali durante il moto, insieme agli effetti opposti connessi al processo di consolidazione (dissipazione), sono trascurati nelle relazioni empiriche convenzionali e nei modelli disponibili in letteratura.

L'importanza degli effetti di queste peculiarità è sottolineato dall'analisi di alcuni casi documentati (colate di Quindici e Guanling) e di misure in laboratorio. Le analisi svolte consentono di validare il modello proposto e dimostrano che i fattori introdotti (i.e. curvatura della superficie di scorrimento, variazione di massa) permettono una migliore interpretazione dei fenomeni considerati.

I principali limiti del modello proposto riguardano la geometria semplificata del corpo della massa granulare in moto (forma parallelepipeda) e della superficie di scorrimento (curvatura della superficie di base soltanto nel piano verticale), l'assegnazione della legge $u_b(t)$, le ipotesi di consolidazione monodimensionale e comportamento elastico-lineare del materiale del versante.

## ABSTRACT

The design of appropriate mitigation measures to protect from landslides require the knowledge of the physical and mechanical processes governing their propagation. This knowledge can derive from experience, carefully verified and modeled through specific rheological models that take into account the main physical and mechanical properties referred to normal stream flows, hyperconcetrated flows, mudflows, debris flows, rock avalanches and their multiphase nature (flow like or granular).

To predict the speed evolution and distance travelled by fine-grained material flows, an analytical (sliding block) model is proposed. The model takes into account (i) the (curved) geometry of the sliding surface; (ii) the mass variation due to possible erosion or deposition processes; iii) the interstitial pressures and, in particular, the evolution of the excess pore water pressures (generation, initially due to several phenomena and during the motion to the slope curvature, coupled to undrained and oedometric conditions; dissipation, due to consolidation process).

The governing ordinary differential equation has been numerically solved. The role played by the main model parameters on the kinematics of rapid fine - grained material flows is evaluated through parametrical analyses and the range of their admissible values is investigated and defined. Model validations using laboratory measurements and analysing some documented cases are finally developed and carried out.

***Keywords**: landslides, rheological models, fine-grained material flows, excess pore water pressure, consolidation, mass variation*

## INTRODUCTION

Landslides consist in the mobilization and sliding along slopes and mountain streams of fluid or granular masses due to the gravity force. Several triggering factors may act: heavy rainfall, earthquakes, temperature changes, human activities.These phenomena can exhibit strongly different mechanical behaviours, affecting their propagation. More specific terminology is needed.

Several classifications of different landslides have been proposed (Varnes, 1978; Davies, 1988; Pierson & Costa, 1987; Coussot & Meunier, 1996). Most of them distinguish between newtonian and non-newtonian flows. Newtonian flows exhibit by a 'fluid' behaviour (e.g. normal stream flows); non-newtonian flows include hyperconcetrated flows, mudflows, debris flows, rock avalanches or sturzstroms, characterized by a 'granular' behaviour, with interstitial fluid consisting of water and suspended fine particles (Pierson & Costa, 1987).

Fine-grained material flows (or rapid mudflows), tipically characterized by a high concentration of silts and clays, are analyzed in the paper; their main geomorphological features are the great travelled distance and the peak velocity, up to 25-30 m/s (e.g. Sarno and Quindici mudflows, 1998).

Their propagation mainly depends on the pore water pressures evolution (Hutchinson, 1986), erosion/deposition processes (Hungr, 2004), as well as on the slope curvature of the sliding surface (De Marchi, 1961; Ciabatti ,1964).

Analytical methods to estimate the distance travelled by granular flows can be usually classified by either sliding block or continuum models.

Sliding block models (Hutchinson, 1986; Ciabatti, 1964) refer to a rigid-body analysis: Hutchinson's model (1986) allows to describe the sliding of fine-grained material flows, affected by an initial excess pore water pressure dissipated during the motion along planar surfaces; Ciabatti's model allows to describe the motion of dry granular flows along curved surfaces, represented by an arc of circumference. Mass variation processes (erosion and deposition) are neglected.

Continuum models are based on the principles of continuum mechanics. These models are numerically implemented; the code FLO 2D (e.g., Peng & Lu, 2012) requires topographic database (e.g. digital elevation model, DEM) and inflow flood hydrographs (not always available) as input data; the code simulates the propagation of mudflows by predicting viscous fluid motion as function of sediment concentration; a quadratic rheologic model (O'Brien & Julien, 1985) for predicting viscous and yield stresses as function of sediment concentration is applied; as sediment concentration changes for a given grid element, dilution effects, mudflow cessation and the remobilization of deposits are simulated. For each grid cell, volume concentration, flow velocity, discharge and flow depth are provided during all times in the simulation. Excess pore pressures and their evolution along the motion are neglected.

Since sliding block models allow to obtain realistic results (Miao *et alii*, 2001; Park *et alii*, 2013), on the basis of simplified models available in literature, a more general sliding block model is proposed, to study the coupled effects of (excess) pore water pressures evolution, as well as the curvature of the sliding surface and the mass variation processes on the kinematics of fine – grained materials flows.

The research – carried out through parametrical computations and back analyses – aims to: a) assess the influence on the runout length by the excess pore water pressure evolution, geometry of the sliding surface, variation of mass; b) test its better capability in mobility prediction with respect to currently available formulations, accordingly to additional introduced parameters or factors (slope curvature and rate of mass change).

## MAIN RHEOLOGICAL LAWS FOR FLUID AND GRANULAR FLOWS

The rheological behaviour of fluid and granular flows (e.g. normal stream flows, hyperconcetrated flows, mudflows, debris

flows, rock avalanches) can be generally described through the following relationship (O'Brien & Julien, 1988):

$$\tau = \tau_c + \tau_{mc} + \tau_v + \tau_t + \tau_d \quad (1)$$

$\tau_c$ being the cohesion between particles; $\tau_{mc}$, the shear stress related to the basal friction (depending on the effective stress σ'); $\tau_v$, the shear stress according to Bingham model; $\tau_t$, the turbulent shear stress; $\tau_d$, the shear stress associated with dispersive pressures (Bagnold).

The role of these shear stresses depends on the nature ('fluid like' or granular) and physical properties (grains' sizes, pore water pressures…..) of the sliding granular mass.

Eq. (1) can be rewritten in terms of gradient of velocity $\delta v/\delta \bar{z}$ ($\bar{z}$ is the direction orthogonal to the sliding surface) (O'Brien & Julien, 1987):

$$\tau = \tau_y + \mu_b \frac{\partial v}{\partial \bar{z}} + \left(\mu_c + \mu_t\right) \cdot \left(\frac{\partial v}{\partial \bar{z}}\right)^2 \quad (2)$$

$\tau_y$ being the shear stress according to Mohr-Coulomb resistance law ($\tau_c + \tau_{mc}(\sigma')$); $\mu_b$, the dynamic viscosity of Bingham; $\mu_c$, a 'dispersive' parameter, expressed as (Bagnold, 1954):

$$\mu_c = a_i \rho_s \lambda^2 d_p^2 \quad (3)$$

$a_i$ is the Bagnold coefficient (= 0.24 for $\lambda \in [14; 17]$ or 0.042 for $\lambda > 1$); λ is the linear concentration ($\lambda = 1/[(c_{max}/c_{vol})^{1/3}-1]$, with $c_{vol}$, volume concentration and $c_{max}$ its maximum value, equal to 0.74 for spherical particles); $\rho_s$, density of solid phase; $d_p$, representative grains' diameter ($\equiv d_{50}$).

$\mu_t$ is the turbulent parameter (generally smaller than $\mu_c$), espressed as:

$$\mu_t = \rho_s l_m^2 \quad (4)$$

with $l_m$ mixing length by Prandtl (Julien & Lan, 1991).

Referring to eq. (2), for normal stream flows, it is possible to assume: $\tau_y(\sigma') = 0$, $\mu_c = \mu_t = 0$, i.e. normal stream flows are characterized by a 'fluid' behaviour, typic of newtonian flows ($\mu_b = \mu_f$ = dynamic viscosity of interstitial fluid).

Hyperconcentrated flows, for low velocity, exhibit a pseudo-plastic behaviour (Nemec, 2009), affected by viscous forces; for high velocity, they characterized by a non newtonian, turbulent behaviour (Smith, 1986): $\mu_b = \mu_c = 0$.

For viscous slurry flows, it can be assumed: $\mu_t = \mu_c = 0$. Mudflows, affected by low velocities, belong to this type of flows (Julien & Paris, 2010). According to Pierson & Costa (1987), for inertial slurry flows at high rates, the viscous behaviour can be neglected because the collisional/dispersive regime becomes dominant. Since these flows are composed by fine-grained materials, the collisional/dispersive regime can be neglected (Federico & Cesali, 2015; 2016). This result can be also confirmed through the evaluation of Bagnold number ($N_{Ba}$), which allows to classify the granular flows according to dominant rheological behaviour (Bagnold, 1954): in particular, if $N_{Ba}<40$, the materials flow is affected by a macro-viscous regime; if $N_{Ba}>450$, by an inertial-granular (collisional) regime; if $40 < N_{Ba} < 450$, by an intermediate regime:

$$N_{Ba} = \frac{\sqrt{\lambda}\rho_s d_p^2}{\mu_f} \frac{\partial v}{\partial \bar{z}} \quad (5)$$

$\mu_f$ is the dynamic viscosity of interstitial fluid (ϵ [0.1; 3] Pa·s, for mudflows, Widjaja *et alii,* 2014).

The inertial-granular (collisional) regime develops within a thin layer, shear layer, at the base of rapid sliding granular masses (Hungr, 1995; Federico & Cesali, 2015; 2016); if a linear change of velocity along the direction orthogonal ($\bar{z}$) to the sliding surface is assumed, the gradient of velocity $\delta v/\delta \bar{z}$ can be expressed as: $v_m/s^s$ ($s^s$ = shear layer thickness; $v_m$ = average value of flow velocity). If $s^s = 4\% \cdot \bar{h}$ (Huang 2003; Liu & Huang, 2006), with $\bar{h}$ flow depth, and $c_{vol} = 0.60$ (Armanini *et alii*, 2003), the Bagnold number ($N_{Ba}$), fixed $v_m$ and $\bar{h}$, by varying $d_p$, assumes the following values (Fig. 1).

It is observed that, for some documented cases of fine grained material flows (Hutchinson, 1986; Zic *et alii*, 2015; Macedonio & Pareschi, 1992; Crosta & Dal Negro 2002), the Bagnold number assumes smaller values than 50, i.e. the macro-viscous regime, characterized by friction and fluid viscosity, is dominant (Fig. 1). Furthermore, fluid viscosity can be neglected for high values of flow velocity and grains' diameter. Moreover, according to Pierson & Costa (1986), slurry flows are often affected by excess pore water pressures; thus, fine-grained material flows, analyzed in the paper, can be associated with these flows but, differently from the original classification proposed by Pierson & Costa (1986) (i.e. inertial slurry flows), they are not characterized by a collisional regime.

For high speed debris flows or avalanches, it is generally assumed: $\mu_b = \mu_t = 0$. Peculiar composition of the sliding debris material (Armanini *et alii*, 2003, Armanini, 2008; 2010; 2013), the relative motion at high rates, as well as grains' collisions within the shear layer, causing 'fluidification' (Hungr & Evans, 1996) and energy dissipation effects, impose the development of specific rhelogical models taking into account laws usually adopted in geotechnical engineering (e.g. Mohr-Coulomb resistance law) and in porous media mechanics (e.g. Collisional Theory by Bagnold), different from the rheological laws generally applied to fluid and granular flows (e.g. Newton and Bingham models). In a rapid granular mass running along mountain streams, normal and shear stresses, associated with a friction regime and a collisional regime, simultaneously occur (Zhang & Foda, 1999; Armanini e*t alii*, 2008; Federico & Cesali, 2015; 2016). Thus, the following rheological law can be reasonably assumed (Federico & Cesali, 2015; 2016):

$$\tau_{max} = \bar{r}_s \tau_{fr} + r_s \tau_{disp} \quad (6)$$

$\tau_{fr}$ is the shear stress associated with frictional regime ($\tau_{fr}(\sigma')$); $\tau_{disp}$, is the dispersive shear stress (Bagnold, 1954); $r_s$ and $\bar{r}_s$ (= 1 - $r_s$) are functions depending on flow velocity (ϵ [0,1])

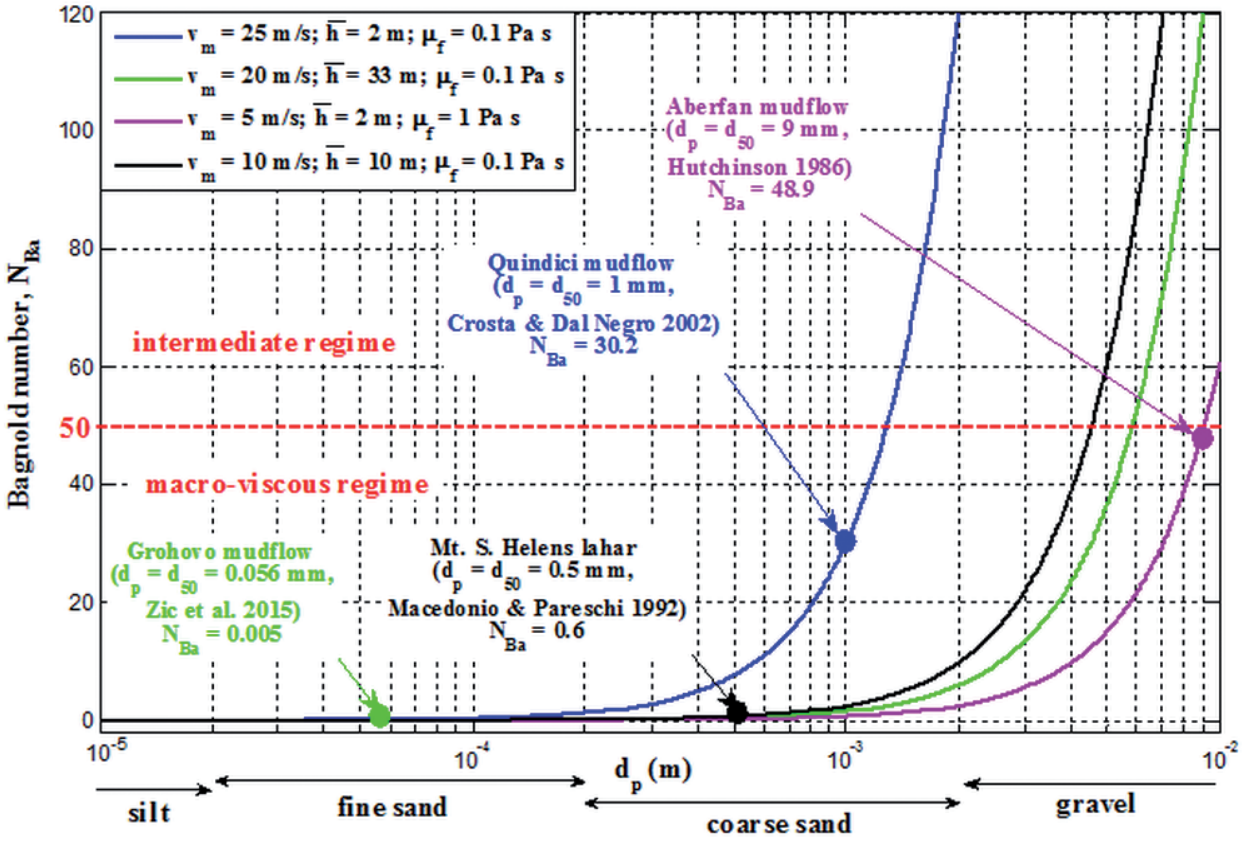


*Fig. 1 - Bagnold number ($N_{Ba}$) vs representative grains' diameter ($d_p$)*

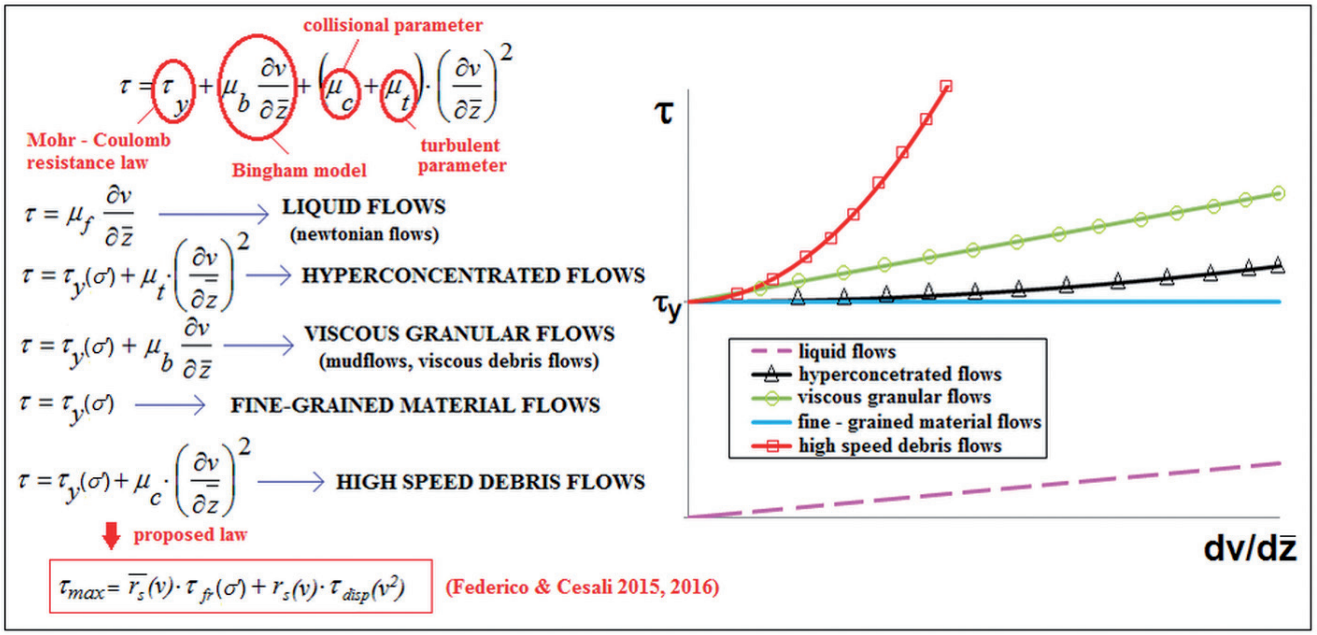


*Fig. 2 - Rheological models for fluid and granular flows*

allowing a "weighted" balance of the basal resistance force ($T_{max}$) according to $\tau_{fr}(\sigma')$ and $\tau_{disp}$, simultaneously acting along an irregular surface. In Fig. 2, previously described rhelogical models for fluid and granular flows are schematically and graphically shown.

## FINE-GRAINED MATERIAL FLOWS

The triggering mechanisms and successive sliding/propagation of fine-grained material flows considerably depend on the excess pore water pressures (Hutchinson & Bhandari, 1971), followed by a consolidation process.The excess pore water pressures can be generated by (i) shear strains induced by an earthquake; (ii) deposition under own weight of granular masses, initially liquefied (Federico & Cesali, 2017); (iii) rapid accumulation of rainwater in soil layers affected by a low permeability; (iv) seepage flow in boundary materials; (v) redistribution of the total stresses caused by internal mechanisms of rupture or reactivation (Comegna & Picarelli, 2005); (vi) compressive deformation of flow body associated with local variation in the slope of the sliding surface or due to a centrifugal force acting along a curvilinear path (De Marchi, 1961; Siviglia & Cantelli, 2005); (vii) consolidation processes under oedometric and undrained conditions (Lambe & Whitman, 1969).

The considerable shear strength reduction, due to the generation of the excess pore water pressures, is often the main reason of slope failures and high mobility of unstable material volumes, even on very gentle slopes; high pore water pressures can also induce the partial or complete liquefaction of the soil (Iverson *et alii*, 1997; Take & Beddoe, 2014).

Conversely, the consolidation process of fine-grained materials along the motion may progressively reduce the pore water pressures and the corresponding increase of the shear strength reduces the travelled distance.

Generally, the kinematics of granular flows can be also remarkably influenced by mass variations ($m$) due to erosion or deposition processes; erosion phenomena may occur along the channel bed or the erodible lateral surfaces (Hungr, 2004). Typically, the erosion phenomenon (mass rate $\dot{m} > 0$) mainly occurs at high elevation, induced by the high slope (up to critical erosion angle $\beta_e$) and the great travel speed, causing strongly increments of the involved volume; while the deposition ($\dot{m} < 0$), caused by the slowdown due in turn to the reduction of slope, downstream occurs.

### *Qualitative description of the motion of fine-grained material flows*

If the sliding surface is represented through two planar surfaces ($x$ = planar abscissa; $\alpha_1$ = first slope; $L_1$ = length of first slope; $\alpha_2$ = second slope or counterslope, Fig. 3a) linked by an arc of circumference ($s$ = curvilinear abscissa; $r$ = curvature radius; $\alpha(s)$ = slope along the curved path = $\alpha_1 - s/r$, Fig. 3a), the rapid fine-grained material flow can be described through the analysis of the following sliding phases (Fig. 3):

a) $t < 0$: the granular mass is initially stable;

b) $t = t_0 = 0$: the excess pore water pressure is generated (a trapezoidal initial excess pore water pressure distribution within a basal saturated layer is assumed) and the mass becomes unstable and starts its runout;

c) $t = t_1 > t_0$: the mass runs along the first slope ($\alpha_1$, $x \in [0, L_1]$, $\dot{x} \neq 0$, $\ddot{x} > 0$) and the consolidation process simultaneously occurs according to physical ($k$, permeability coefficient), mechanical ($E_{ed}$, oedometric modulus) and geometrical ($H$, drainage length) parameters of involved materials; mass variation ($\dot{m} \lessgtr 0$ if $\alpha_1 \lessgtr \beta_e$) processes can also occur;

d) $t = t_2 > t_1$: the mass begins to run along the curved path ($x = L_1$; $s = 0$; $\alpha(s=0) = \alpha_1$); total normal stress increase due to centrifugal force ($\Delta N \sim \dot{x}^2$), pore water pressure increments due to curvature of the flow lines ($\Delta p_{w,b,k} \sim \dot{x}^2$) and $\Delta N$ under undrained and almost oedometric conditions ($\Delta p_{w,b,\Delta N} \sim \Delta N/\Omega$, $\Omega$ = basal area) occur at the base of the sliding mass;

e) $t = t_3 > t_2$: the mass runs along the curved path ($s \in [0, r\cdot(\alpha_1-\alpha_2)]$); the consolidation and mass variation ($\dot{m} \lessgtr 0$ if $\alpha_2 \lessgtr \beta_e$) processes simultaneously occur; the previous increments of the total normal stress ($\Delta N$) and pore water pressures ($\Delta p_{w,b,k}$, $\Delta p_{w,b,\Delta N}$) due to slope curvature as well as to the undrained (full or partial) conditions increase according to the current velocity ($v = \dot{x}$) of the sliding mass;

f) $t = t_4 > t_3$: the mass begins to run along the second slope ($\alpha(s) = \alpha_2$, $s=r\cdot(\alpha_1-\alpha_2)$); the consolidation and mass variation ($\dot{m} \lessgtr 0$ *if* $\alpha_2 \lessgtr \beta_e$) processes simultaneously occur; the velocity of the mass at the beginning of the second planar surface strongly depends on the increments (positive or negative) of the pore water pressures occurred during the previous two (first planar and curved) surfaces;

g) $t = t_5 > t_4$: the mass decelerates along the second slope ($\alpha_2$, $\ddot{x} < 0$); the consolidation and mass variation ($\dot{m} \lessgtr 0$ *if* $\alpha_2 \lessgtr \beta_e$) processes simultaneously occur;

h) $t = t_6 > t_5$: the mass stops its runout ($v = \dot{x} = 0$; $x = x_{max}$ = runout length).

### *Analytical description of the motion of fine-grained material flows*

**Geometry**

It is analyzed the motion of a fine-grained material block of thickness $\bar{h}$ and length $b$ (Fig. 4, 1 m length along the direction orthogonal to the slope, $\Omega = b \cdot 1$). The slope $\alpha$ of the sliding surface may generally decrease or increase along its curved path ($s$ = curvilinear abscissa, $r$ = curvature radius). The sliding surface (*s.s.*) can be schematized through: a) an arc

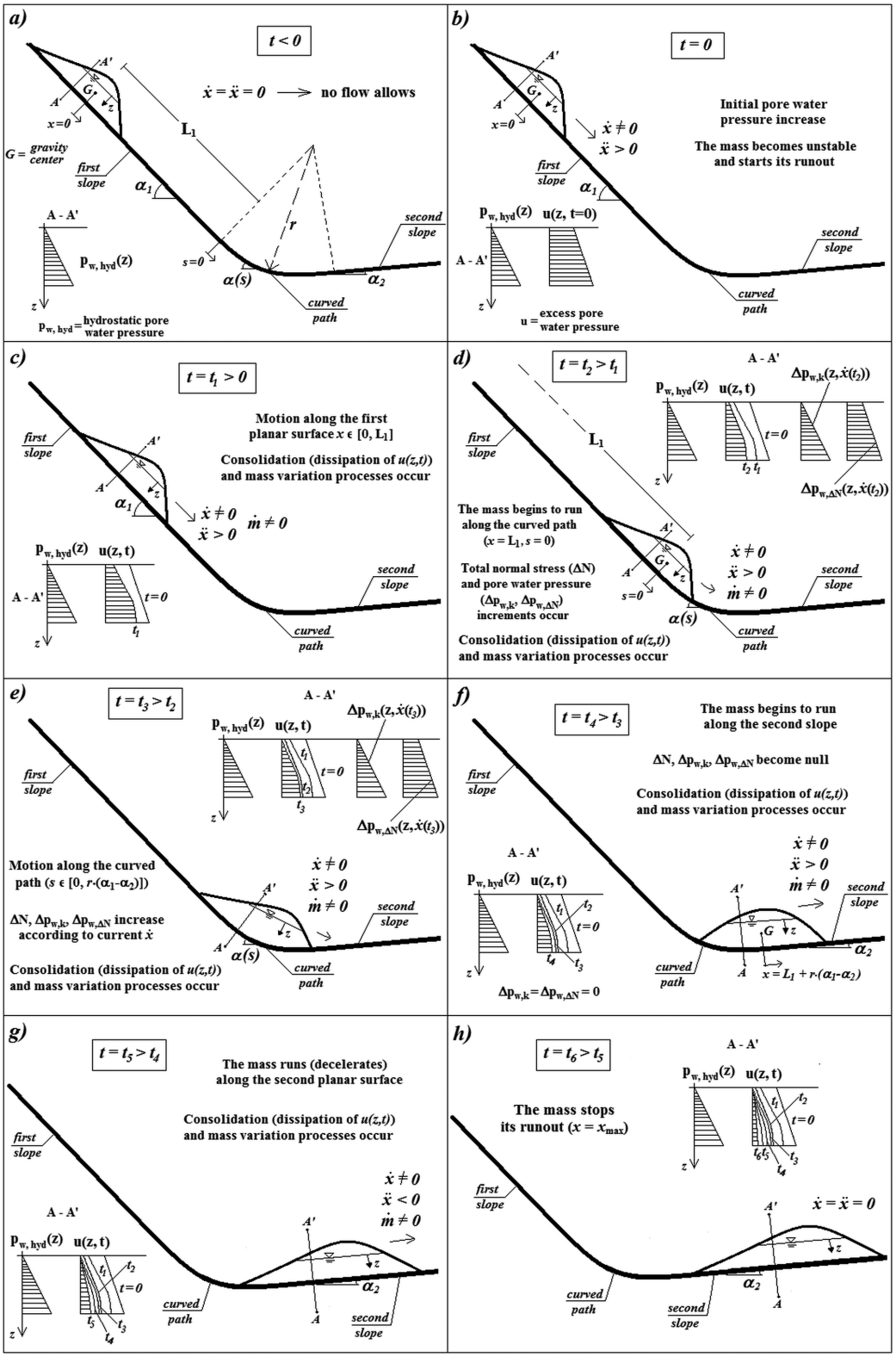


*Fig. 3 - Sliding phases of a fine-grained material flow*

of circumference; b) two planar surfaces linked by an arc of circumference ($1/r \neq 0$ starting by $s = 0$); c) two planar surfaces, i.e. r → ∞ (Fig. 5).

**Pore water pressures**

It is assumed a trapezoidal initial pore water pressure distribution ($p_w(z)$) within a basal layer of thickness $S\bar{h}$ ($S$ = percentage of saturated layer ϵ [0,1]) (Fig. 4). The initial values $p_{w,t0}$ and $p_{w,b0}$ of pore water pressure, at the top and the base of the saturated layer, depend on the values of hydrostatic interstitial pressure ($p_{w,hyd}(z)=\gamma_w\, z\, cos\, \alpha$) and on the excess pore water pressure $u(z,t)$ ($z$, normal to the sliding surface, directed downward, from the upper surface of the saturated soil layer, Fig. 4). The resultant $U$ of the pore water pressures at the base of the sliding mass ($p_{w,b}(t)$) is equal to the sum of the basal hydrostatic interstitial pressure ($p_{w,hyd}(z=S\bar{h})=p_{w,b,hyd}$) and the basal excess pore water pressure at time $t$ ($u(z=S\bar{h},t)=u_b(t)$):

$$U = p_{w,b}(t)\, b = [p_{w,b,hyd} + u_b(t)]\, b \qquad (7)$$

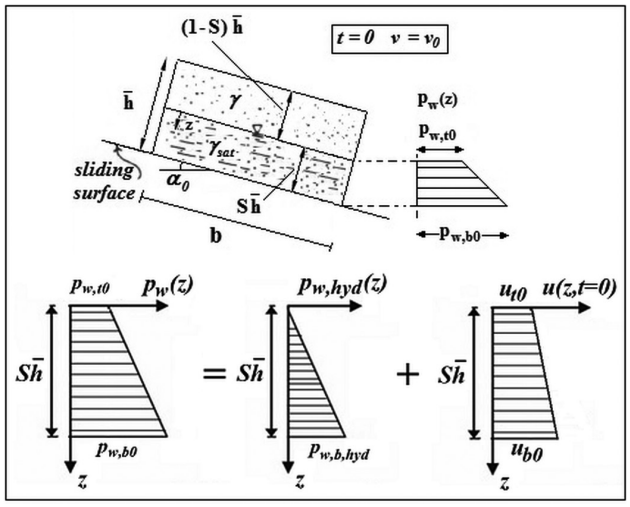


*Fig. 4 - Geometry of the sliding mass and assumed initial pore water pressure distribution*

**Dissipation of the excess pore water pressure**

The evolution of the excess pore water pressure, at the base of the sliding granular mass, is simply described through the following dissipation law $u_b(t)$, which approximates the solution of the 1-D consolidation equation by Terzaghi & Frohlich (1936), referred to the case of impermeable horizontal base and drainage only through the upper surface of the saturated soil layer, for an initial trapezoidal excess pore water pressure distribution (Federico & Cesali, 2017):

$$u_b(t) = u_{b,0}\, e^{-at} \qquad (8)$$

$u_{b0}$ ($= u(z=S\bar{h},\ t=0)$) is the initial basal excess pore water pressure; $a$ is a parameter related to the variables that govern the consolidation process of the involved material.

The excess pore water pressure may induce soil liquefaction (Take & Beddoe 2014), generally describing a condition for which the pore water pressures produce negligible effective stresses in a soil mass (Iverson *et alii*, 1997; Major, 2000). The condition for liquefaction requires therefore that the pore water pressure ($p_w$) equals the total normal stress (σ):

$$p_w(z) = p_{w,hyd}(z) + u(z,t) \equiv \sigma(z) = \left[\gamma \bar{h} \cdot (1-S) + \gamma_{sat} z\right] \cdot \cos\alpha \qquad (9)$$

γ being the unit weight of the unsaturated layer of thickness $(1\text{-}S)\bar{h}$; $\gamma_{sat}$, the unit weight of the saturated layer of thickness $S\bar{h}$ ($\gamma_{sat}=\gamma'+\gamma_w$, with $\gamma'$ = soil effective weight; $\gamma_w$ = unit weight of water).

Since the effective normal stress $\sigma' = \sigma - p_w$ (Terzaghi's criterion), eq. (9) implies that $\sigma' = 0$ everywhere in the soil mass and that the frictional strength of the soil is zero. If strength due to cohesion is also negligible, soils in which eq. (9) is satisfied can flow quite readily, like a liquid. Furthermore, since the basal hydrostatic interstitial pressure is expressed as:

$$P_{w,hyp}(z=S\bar{h}) = p_{w,b,hyp} = \gamma_w\, S\bar{h}\, cos\, \alpha \qquad (10)$$

eq. (9) (for $z=S\bar{h}$) implies that the initial basal excess pore water pressure $u_{b0}$ must be smaller than the maximum value $u_{b0,max}$:

$$u_{b0,max} = [(1-S)\,\gamma + S\gamma']\, \bar{h}\, cos\, \alpha \qquad (11)$$

Thus, the initial basal pore water pressure $u_{b0}$ can be expressed as follows:

$$u_{b,0} = r_{0,b}\, u_{b0,max} \qquad (12)$$

where the coefficient $r_{0,b}$ ($= u_{b0}/u_{b0,max}$) is defined as the ratio between the current initial excess pore water pressure at the base of the granular mass and its maximum value (Hutchinson, 1986); $r_{0,b} \leq 1$ must be assigned to avoid the occurrence of the initial soil liquefaction and to apply the proposed model.

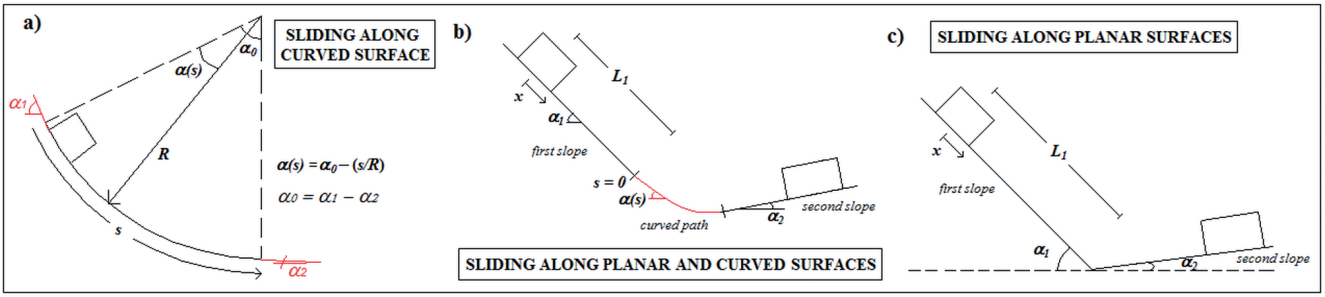


*Fig. 5 - Possible geometries of the sliding surface*

**Law of motion**

The mass ($m$) of the sliding block may vary along its motion due to erosion/deposition processes. In this general condition, the law of motion is expressed as follows:

$$mg \sin \alpha - \left[ N - (p_{w,b,hyd} + u_b(t) \cdot b \right] \cdot \tan \varphi' = m(t) \frac{dv(t)}{dt} + v(t) \frac{dm(t)}{dt} \quad (13)$$

$v$ being the velocity of the block; $w^*$, the velocity of the incorporated or lost mass. The resultant $F$ of forces acting on the block (Fig. 6) is expressed as follows:

$$F = mg \sin \alpha - T_{max} \quad (14)$$

$g$ being the gravity acceleration; $\alpha$, the angle of slope of the sliding surface; $T_{max}$, the shear resistance force (neglecting cohesion and considering the basal resistance law purely frictional):

$$T_{max} = (N - U) \tan \phi' \quad (15)$$

$\varphi'$ being the shear resistance angle along the basal surface; $N (= mg \cdot \cos\alpha)$, the resultant of the total normal stresses at the base. The possible variation of the friction angle $\varphi'$ with the velocity (Fukuoka, 1991; Wang *et alii*, 2010; Miao *et alii*, 2014), occurring at the base of sliding granular materials, is neglected. According to several Authors, there are no appreciable rate effects on the friction angle in (coarse, fine and saturated) sandy materials (Novosad, 1964; Scarlett & Todd, 1969; Hungr & Morgenstern, 1984) and in low clay fraction soils (Skempton, 1985). Conversely, shear tests on clays at fast rates (e.g. 800 mm/min) show changes in shear strength, probably associated with a rearrangement of the originally ordered structure or, if the dissipation is not allowed, also the possible pore water pressure generation (Skempton, 1985). Furthermore, in shear ring tests on samples of materials involved in rapid landslides (Fukuoka, 1991; Tika & Hutchinson, 1999), opposite (positive and negative) rate effects on shear strength were observed. Thus, more detailed research is needed to better define the limits of this phenomenon and to explore the effects at faster rates, maybe typical of granular flows. The energy dissipation due to grains collisions, mainly occurring in debris flows or avalanches, can be neglected for fine-grained materials (Federico & Cesali, 2015, 2016).

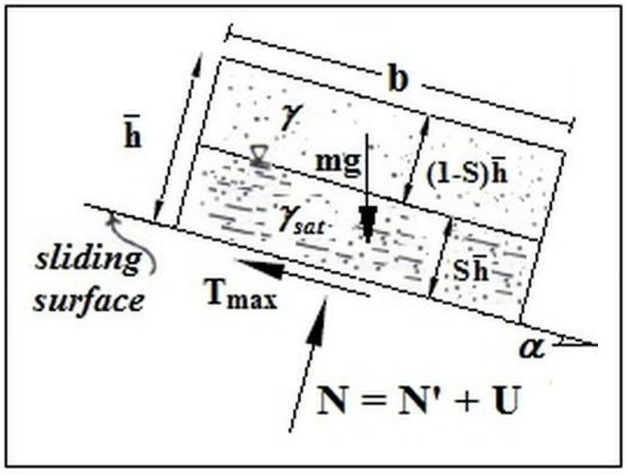


*Fig. 6 - Forces acting on the sliding block*

If the rate $w^*$ is assumed null (Van Grassen & Cruden, 1990), eq. (13) can be finally rewritten as:

$$mg \sin \alpha - \left[ N - (p_{w,b,hyd} + u_b(t) \cdot b \right] \cdot \tan \varphi' = m(t) \frac{dv(t)}{dt} + v(t) \frac{dm(t)}{dt} \quad (16)$$

In more general cases, the law of motion (eq. (16)) must be rewritten by taking into account the effects of the curvature of the sliding surface (Federico & Cesali, 2017).

**Effects induced by the curvature of the sliding surface**

If the sliding surface is affected by a curvature $1/r \neq 0$, the centripetal force $(= m \cdot s^2/r(s) = m \cdot v^2/r(s))$ occurs; this force modifies the normal resultant forces $N$ and $U$ and the global shear resistance force $T_{max}$. The reduction in the slope of the sliding surface $\alpha(s) = \alpha_0 - s/r$ ($\alpha_0$ is the slope of the sliding surface at the beginning of the curved path) induces the decrease of the driving force ($= m\, g \sin \alpha(s)$ ) and the increase of $N$. Therefore, the current value of the total normal force acting at the base of the sliding mass is expressed as follows:

$$N = mg \cos \alpha + m\,(v^2/r) \quad (17)$$

where it is clearly recognizable that the increase $\Delta N = m \cdot v^2/r$ is associated with the curvature of the sliding surface and the velocity of the sliding mass. Furthermore, if the curvature assumes high values, the pore water pressure doesn't vary hydrostatically (De Marchi, 1961; Siviglia & Cantelli, 2005): the change of the direction of motion of a fluid particle (curvilinear path) induces an increase of the piezometric head and interstitial pressures (Fig. 7a):

$$p_w(z) = \Delta p_{w,hyd}(z) + \Delta p_{w,k}(r(z),z) \quad (18)$$

with

$$\Delta p_{w,k}(r(z),z) = \gamma_w \frac{v^2}{r(z) g} z \quad (19)$$

$\Delta p_{w,k}(r(z),z)$ being the increment of pore water pressure due to the curvature of the sliding surface; $r(z) = r_b - \bar{h} + z$; $r_b$ = curvature radius at the base of the sliding block ($r = r_b$, for shallow flows). According to above equations, it is possible to write (Fig. 7 a, Siviglia & Cantelli, 2005):

$$\frac{p_w(z)}{p_{w,b,hyd}} = \frac{z}{\bar{h}} \cdot \left[ 1 + \Psi(r(z),z) \right] \quad (20)$$

being

$$\Psi(r(z),z) = \frac{\Delta p_{w,k}(r(z),z)}{p_{w,b,hyd}} = \frac{v^2}{r(z) g \cos \alpha} \quad (21)$$

If $r >> \bar{h}$ (i.e. for shallow flows), the increment of the pore water pressure (eq. (19)) can be neglected if compared with the hydrostatic one (Fig. 7a).

An additional coupled effect related to the curvature of the sliding surface arises, expecially for fine grained soils (small $c_v$

values), if the increase of total normal stresses $\Delta\sigma_{\Delta N}$ in the saturated mass and the 'almost' undrained condition, that may take place during the short interval time elapsing during the curved path, are taken into account. If elastic mechanical behaviour of the saturated mass is assumed, an additional pore water pressure increase could arise and, therefore, must be considered (Lambe & Withman, 1969):

$$\Delta p_{w,\Delta N} = C_{pw}\,\Delta\sigma_{\Delta N}(z) \tag{22}$$

with

$$\Delta\sigma_{\Delta N}(z) = \gamma(1-S)\bar{h}\frac{v^2}{rg} + \gamma_{sat} z\frac{v^2}{rg} \tag{23}$$

$C_{pw}$ (generally equal to 1 for saturated materials) being the pore water pressure parameter for loading processes under oedometric and undrained conditions (Lambe & Whitman, 1969). At the base ($z = S\bar{h}$) of the sliding mass, eq. (19) and eq. (23) can be rewritten as follows:

$$\Delta p_{w,b,k} = \gamma_w \frac{v^2}{r(z)g} S\bar{h}\,; \quad \Delta p_{w,b,\Delta N} = C_{pw}\cdot\Delta\sigma_{b,\Delta N}$$

$\Delta\sigma_{b,\Delta N}$ being the increase of basal total normal stresses ($\Delta\sigma_{\Delta N}$ $(z=S\bar{h})$).

The comparison between the computed increments $\Delta p_{w,b,k}$ and $\Delta p_{w,b,\Delta N}$, for a saturated soil ($S = 1$), is shown in Fig. 7b: for small values of the radius $r$ (e.g. 100 m), a remarkable difference between $\Delta p_{w,b,k}$ and $\Delta p_{w,b,\Delta N}$ is observed; for high values of $r$ (e.g. 2000 m), $\Delta p_{w,b,k}$ and $\Delta p_{w,b,\Delta N}$ become comparable. Under these assumptions, the resultant $U$ of the pore water pressure at the base of the sliding mass ($p_{w,b}$) should be rewritten as follows:

$$U = \left[ p_{w,b,hyd} + u_b(t) + \Delta p_{w,b} \right]\cdot b \tag{24}$$

being $\Delta p_{w,b} = \Delta p_{w,b,k} + \Delta p_{w,b,\Delta N}$.

Therefore, the global shear resistance force $T_{max}$ (eq. (15)) may be more generally expressed as follows:

$$T_{\max} = \left\{ \left[ mg\cos\alpha(s) + m\frac{v^2}{r} \right] - \left[ p_{w,b,hyd} + u_b(t) + \Delta p_{w,b,k} + \Delta p_{w,b,\Delta N} \right]\cdot b \right\}\cdot \tan\varphi' \tag{25}$$

**Effects induced by the mass variation of the sliding block**

The mass $m(t)$ may be expressed as (Cannon & Savage, 1988):

$$m(t) = m(x(t)) = m_0 + \mu'(x-x_e) \tag{26}$$

$m_0$ (kg) being the initial mass ($= [(1-S)\cdot\gamma + S\cdot\gamma_{sat}]\, b\bar{h}/g$); $\mu'$ (kg/m), the erosion/deposition rate ($\mu' > 0$, erosion; $\mu' < 0$, deposition); $x_e$, the abscissa for which the erosion/deposition process starts; in particular, several authors (Ikeya, 1981; Hungr, 2004) suggested:

$$\mu' = \begin{cases} \mu'_e > 0, & se\ \ \alpha(s) > \beta_e \\ \mu'_d < 0, & se\ \ \alpha(s) < \beta_e \end{cases} \tag{27}$$

$\beta_e$ being the erosion critical slope generally ranging between 8°-14°; $\beta_e$ can also be evaluated through the following relationship (Takahashi, 1991):

$$\beta_e = arctag\left[ \tan\varphi' \cdot \left( 1 - 2\frac{\gamma_w}{\gamma_{bed}} \frac{1}{1+\frac{\gamma^*}{\gamma_{bed}}} \right) \right] \tag{28}$$

$\gamma_{bed}$ being the unit weight of the material lying on the bed of the channel (typically, 18-20 kN/m³); $\gamma^*$ ($= (1-S)\cdot\gamma + S\cdot\gamma_{sat}$), the average (according to factor $S$) unit weight of the sliding granular block.

**Governing equation and conditions**

Under the previous assumptions, eq. (16) describing the sliding of the considered block is rewritten as follows:

$$\ddot{s} + \dot{s}^2\left( \frac{1}{m(s(t))}\frac{dm}{ds} + \left[ 1 - \frac{((1-S)\cdot\gamma + (\gamma_{sat}+\gamma_w)\cdot S)\cdot\bar{h}\cdot b}{g\cdot m(s(t))} \right]\frac{\tan\vartheta}{r(s)} \right) - g\left[ \sin\alpha(s) - \cos\alpha(s)\tan\vartheta \right] - \left[ \left( \gamma_w S\bar{h}\cdot\cos\alpha(s) + u_{b,0}e^{-at} \right)\frac{b}{m(s(t))} \right]\tan\vartheta = 0 \tag{29}$$

$s$ being the curvilinear abscissa; $\alpha(s)=\alpha_0 - s/r$ ($\alpha_0=\alpha(s=0)$).

At time $t=0$, the block starts its sliding along a surface sloped $\alpha=\alpha_0$, with initial speed $v=v_0$.

Eq. (29) may also be formally rewritten as:

$$\ddot{s} + \dot{s}^2 f_1(s) + f_2(s) = f_3(s)\, e^{-at} \tag{30}$$

being

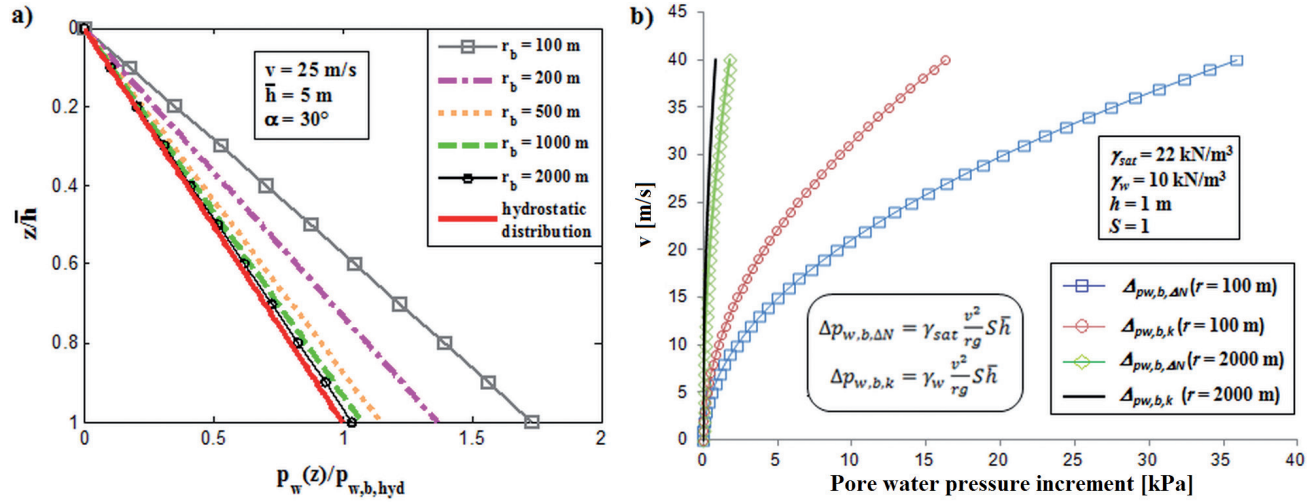


*Fig. 7 - a) Effects of slope curvature on pore water pressure: $z/\bar{h}$ vs $p_w/p_{w,b,hyd}$; b) Comparison between $\Delta p_{w,b,k}$ and $\Delta p_{w,b,\Delta N}$*

$$f_1(s) = \left\{ \frac{1}{m(s(t))} \frac{dm}{ds} + \left[ 1 - \frac{((1-S)\cdot\gamma + (\gamma_{sat} + \gamma_w)\cdot S)\cdot \bar{h}\cdot b}{g\cdot m(s(t))} \right] \frac{\tan\varphi'}{r(s)} \right\} \quad (31)$$

$$f_2(s) = -g\left[ \sin\alpha(s) - \left( 1 - \frac{\gamma_w S \bar{h}\cdot b}{g\cdot m(s(t))} \right) \cos\alpha(s) \tan\varphi' \right] \quad (32)$$

$$f_3(s) = \frac{u_{b,0} b}{m(s(t))} \tan\varphi' \quad (33)$$

## PROPOSED SOLUTIONS AND PARAMETRICAL ANALYSES

Eq. (29) must be numerically integrated. The closed form solution of eq. (29) can be found only if some specific assumptions are considered. In particular, if i) planar sliding surfaces ($r \rightarrow \infty$, Fig. 5c); ii) frictional basal resistance law; iii) constant mass ($\mu' = 0$) are assumed, the motion's law of Hutchinson's model (1986) is obtained:

$$\ddot{x} = g\cdot\{\sin\alpha - [\cos\alpha - (p_{w,b}(t)/\bar{h}\cdot\gamma^*)]\tan\varphi'\} \quad (34)$$

If constant mass ($\mu' = 0$), curved sliding surface ($1/r \neq 0$, Fig. 5a) and dry granular flow ($S = 0$; $p_{w,b} = \Delta p_{w,b} = 0$) are assumed, eq. (29) provides the law of motion proposed by Ciabatti (1964):

$$\ddot{s} + \dot{s}^2 (\tan\varphi'/r(s)) - g\cdot[\sin\alpha(s) - \cos\alpha(s)\tan\varphi'] = 0 \quad (35)$$

Eq. (34), (35) can be simply solved in closed form (Hutchinson, 1986; Ciabatti, 1964; Federico & Cesali, 2017).

Thus, under specific assumptions the proposed model admits as particular solutions the models developed by Hutchinson (1986) and Ciabatti (1964).

The numerical solution of eq. (29) is obtained by applying the Finite Difference Method (FDM); in particular, the governing ordinary differential equation is discretized according to the Eulero method. If the integration time interval assumes small values, the numerical solution becomes more stable, but the computation time increases. In the proposed model, the following value (0.25 s; 0.5 s; 1 s) has been parametrically chosen for the integration time interval.

The proposed model depends on several parameters ($r$, $r_{0,b}$, $a$ or $c_v$, $S$, $\mu'$) pertaining to terrain and flow properties. Terrain properties include the geometry of the sliding surface and the erodibility of the channel bed (initial and final volume/mass of the involved material); flow properties include the dissipation of the excess pore water pressure (and the consolidation phenomena), the runout distance and the flow velocity.

Determination of the model parameters greatly influences reliable forecasts. The admissible values of the main model parameters have been evaluated by using lab experiments and field observations results available in literature and providing relationships linking them to typical physical and mechanical parameters pertaining to the involved materials (Federico & Cesali, 2017).

In particular, the parameter $r_{0,b}$, if the initial basal excess pore water pressure ($u_{b0}$) is generated by cyclic shear stresses, can be evaluated through the relationship reported in Table 1, according to the following parameters: $OCR$ = overconsolidation ratio; $A$ and $B$ = parameters dependent on plasticity index $PI$; $\eta$= an experimental coefficient (suggested value 0.45); $\gamma_{c,max}$, the maximum shear strain, which can be assumed equal to average shear strain $\gamma_{av}$, defined in function of the maximum earthquake-induced acceleration (Federico & Cesali, 2017). If $u_{b0}$ is induced by deposition of consolidating (initially liquefied) mud granular materials, $r_{0,b}$ assumes values approximately ranging between 0.85÷0.95 (Federico & Cesali, 2017).

The parameter $a$ can be evaluated (Fernandez-Merodo *et alii,* 2008; Lollino *et alii*, 2014; Chian, 2015; Federico & Cesali, 2017) through the variables governing the consolidation process of the involved materials (e.g. $H$ = the the maximum drainage distance; $c_v$, = the 1-D consolidation coefficient related to the parameters $E_{ed}$, oedometric modulus, and $k$, permeability coefficient = $k\cdot E_{ed}/\gamma_w$, with $\gamma_w$, unit weight of the water, Tab. 1).

The erosion ($\mu_e'$) rate tipically ranges between $0 \div 9\cdot10^3$ kg/m, approximately (Federico & Cesali, 2017). Absolute value of $\mu_d'$ ($< 0$) is generally assumed equal to $\mu_e'$.

| Parameter | Range of admissible values | Relationships |
|---|---|---|
| $r_{0,b}$ | 0.85 ÷ 0.95 | $r_{b,0} = \eta\cdot\log\frac{\gamma_{c,\max}}{A\cdot(OCR+1)+B}$ |
| $a$ | - | $a = \frac{\pi^2}{4}\frac{c_v}{H^2}$ |
| $\mu_e'$ (= $\lvert\mu_d'\rvert$) | $0 \div 9\cdot10^3$ kg/m | - |

*Tab. 1 - Relationships and admissible values for the parameters $r_{0,b}$, $a$, $\mu'$*

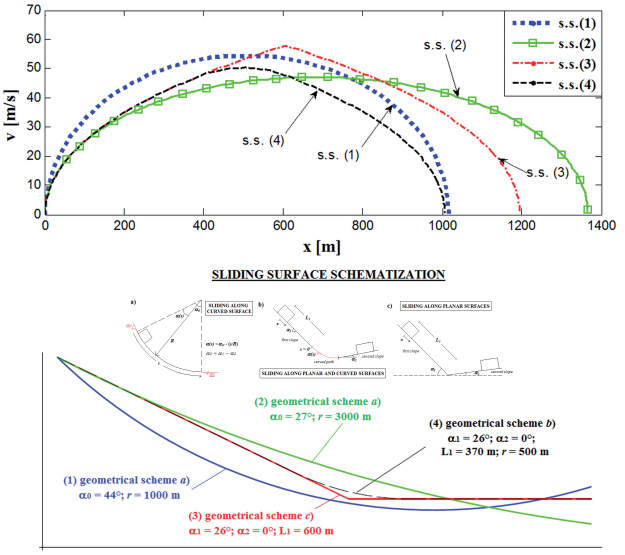


*Fig. 8 - Velocity vs travelled distance for different schematizations of the sliding surface*

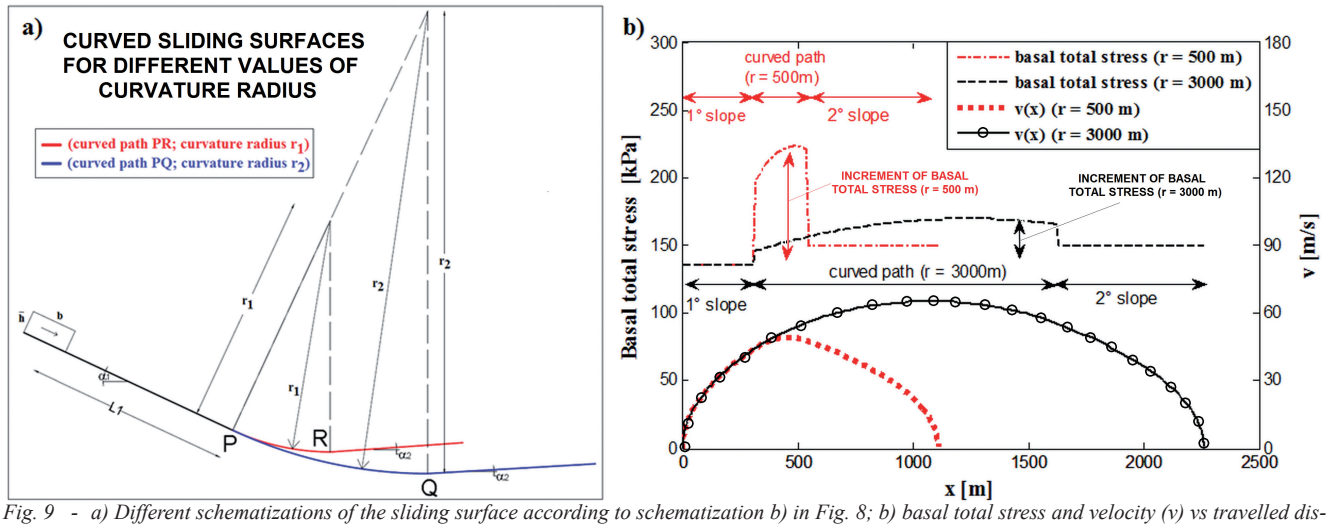


*Fig. 9 - a) Different schematizations of the sliding surface according to schematization b) in Fig. 8; b) basal total stress and velocity (v) vs travelled distance (x) for different values of r*

Therefore, the sensitivity of the proposed numerical solution to these parameters is evaluated, by taking into account their ranges of admissible values, above introduced.

### *Effect of the geometry of the sliding surface*

The influence of the geometry of the sliding surface, on the total runout length and the evolution of the speed of the sliding mass is evaluated. The following parameters are selected: $\phi' = 35°$; $\bar{h} = 10$ m; $b = 50$ m; $S = 0.1$; $r_{0,b} = 0.87$; $\gamma = 14$ kN/m$^3$; $\gamma_{sat} = 19$ kN/m$^3$; $c_v = 0.005$ m$^2$/s (silt), $\mu'_e = \mu'_d = 0$ (constant mass). For the sliding surface, the geometrical schematizations shown in Fig. 8 are considered.

The curvature radius $r$ greatly influences the kinematics of the sliding mass (Fig. 8); if $r$ increases, the traveled distance and the maximum rate increase due to a decrease of the resistance force $T_{max}$. The centrifugal force along the curved path increases the interparticle normal forces and compacts the soil structure, causing a sudden increase of the pore water pressures (De Marchi, 1961, Siviglia & Cantelli, 2005).

Therefore, the effect of the slope curvature on the total and the effective stresses ($\sigma$,$\sigma'$) and the pore water pressure ($p_w$) is investigated (Figs. 9-12). The following input parameters are considered: $\phi' = 35°$; $\bar{h} = 10$ m; $b = 50$ m; $\gamma = 14$ kN/m$^3$; $\gamma_{sat} = 19$ kN/m$^3$; $r_{0,b} = 0.87$; $S = 0.20$; $c_v = 0.01$ m$^2$/s; $\mu'_e = \mu'_d = 0$ (constant mass). The sliding surface is described according to Fig. 9 a (geometrical schematization b), Fig. 5): $\alpha_1 = 25°$; $\alpha_2 = 0°$; $L_1 = 300$ m; $r_1 = 500$ m (curved path $\widehat{PR} \approx 220$ m); $r_2 = 3000$ m (curved path $\widehat{PQ} \approx 1300$ m).

It may be observed that small values of $r$ induce a considerable increase of the basal pore water pressures (Fig. 10), especially of $\Delta p_{w,b,\Delta N}$ (Fig. 11), causing the reduction of the basal effective stresses $\sigma'$ (Fig. 12a) and a more rapid change of

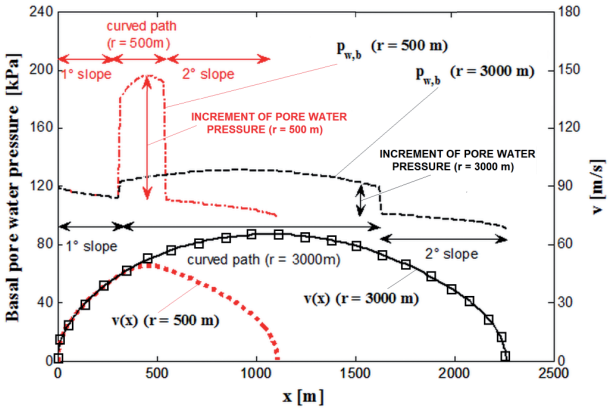


*Fig. 10 - Basal pore water pressure and velocity (v) vs travelled distance (x), for different values of r*

the velocity ($\Delta v/\Delta x$) of the sliding mass along the curved path (Fig. 12b); smaller values of the runout length (for $r = 500$ m) are due to a larger reduction of the slope curvature.

### *Effect of the excess pore water pressure*

The role of the dissipation of the basal excess pore water pressure $u_b(t)$ on the kinematics of sliding fine – grained materials is investigated (Fig. 13). To this purpose, the following parameters are assigned: $\alpha_0 = 28°$; $r = 2000$ m (geometrical schematization a), Fig. 5); $\phi' = 26°$; $\bar{h} = 20$ m; $S = 0.25$; $r_{0,b} = 0.88$; $\gamma = 14$ kN/m$^3$; $\gamma_{sat} = 19$ kN/m$^3$; $\mu'_e = \mu'_d = 0$ (constant mass). If the consolidation coefficient $c_v$ (and then the parameter $a$) decreases, the traveled distance and the maximum rate increase and, in particular, for small values of $c_v$ (corresponding to a silt and clayey silt), the runout length becomes almost independent on $c_v$ and tends to the value obtained assuming $u_b = u_{b0} = constant$ (Fig. 13a).

On the contrary, for values of $c_v$ corresponding to those

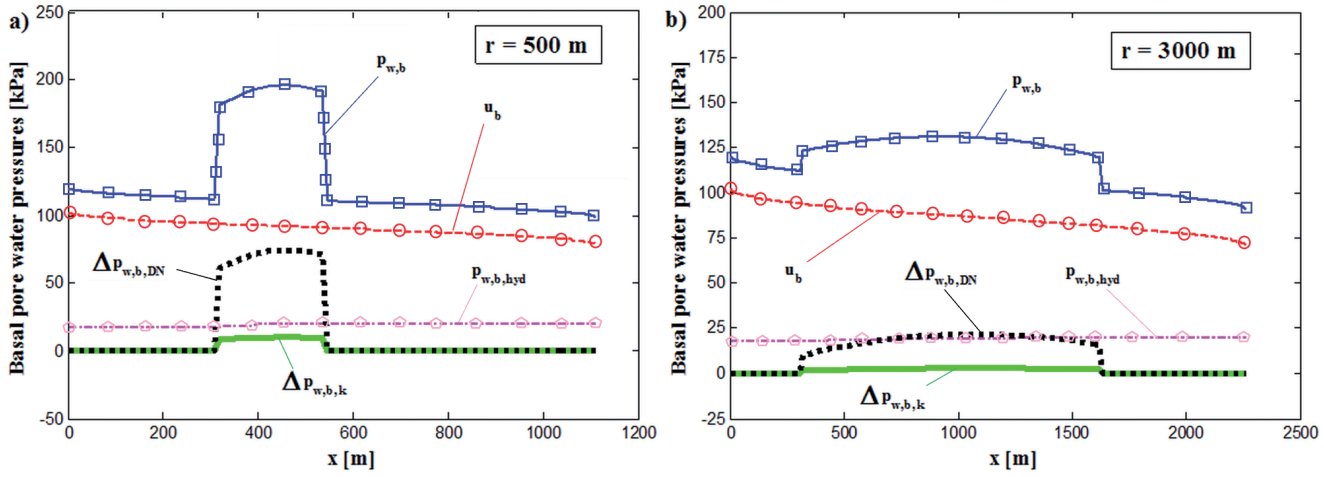


*Fig. 11 - Pore water pressure contributions $p_{w,b}$, $p_{w,b,hyd}$, $u_b$, $\Delta p_{w,b,k}$, $\Delta p_{w,b,\Delta N}$ vs travelled distance (x), for a) r= 500 m; b) r= 3000 m*

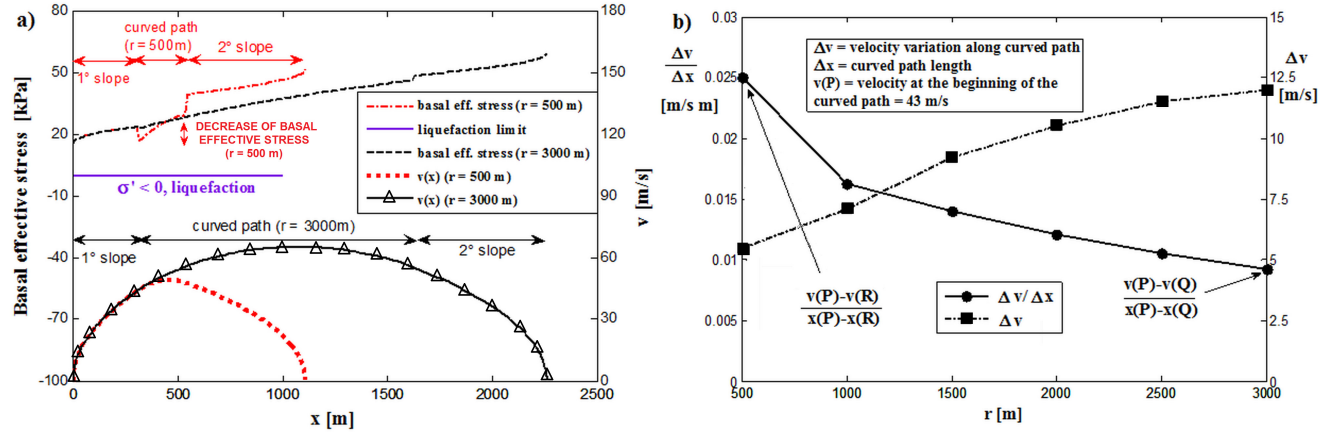


*Fig. 12 - a) Basal effective stress and velocity (v) vs travelled distance (x), for different values of r; b) Δv/Δx and Δv vs r*

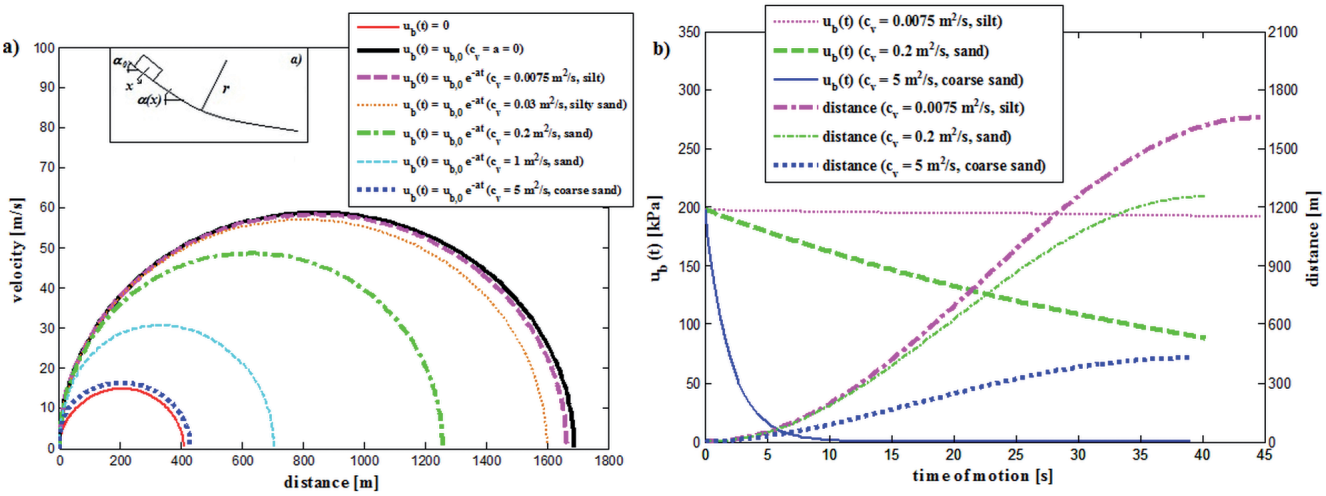


*Fig. 13 - a) Velocity vs travelled distance; b) basal excess pore water pressure ($u_b$) and travelled distance vs time, for different values of consolidation coefficient $c_v$*

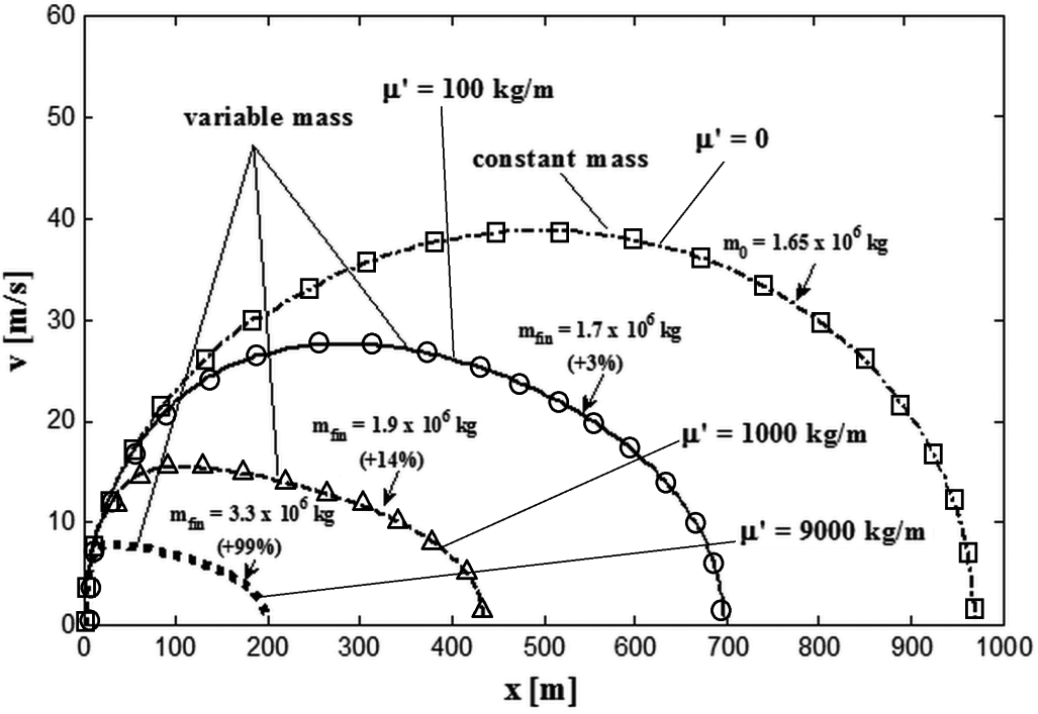


*Fig. 14 - Effect of the variation of the mass: velocity vs runout length*

characterizing a coarse sand, the runout length rapidly tends to the value obtained assuming $u_b = 0$. For materials as silt and clay, the total dissipation of the basal excess pore water pressure occurs for longer time than the duration of the sliding of the granular mass and, thus, the approximate expression $u_b(t) = u_{b,0}$ can be assumed. For more permeable materials, the basal excess pore water pressure is quickly dissipated compared with the duration of motion and it can be neglected (Fig. 13b).

### *Effect of the variation of the mass*

The effect of mass change along the motion of a fine grained material flow is evaluated. By assigning the input parameters: $\alpha_1$ = 20°; r = 1500 m (geometrical schematization a) of the sliding surface, Fig. 5); ϕ' = 25°; $\bar{h}$ = 15 m; $b$ = 50 m; γ = 15 kN/m$^3$; $\gamma_{sat}$ = 22 kN/m$^3$; μ' = $\mu'_e$ = $\mu'_d$ (only erosion); $r_{0,b}$ = 0.87; $S$ = 1; $c_v$ = 0.02 m$^2$/s; $\gamma_{bed}$ = 18 kN/m$^3$, the following results are obtained (Fig. 14). The mass variation greatly influences the kinematics of the sliding block; in particular, if erosion processes occur, the runout length and the maximum rate considerably decrease.

## APPLICATION TO CASE STUDIES

The proposed model has been applied to the following documented cases: Quindici mudflow (Campania, Italia, 1998) and Guanling landslide (China, 2010), as well as to the back analysis of experimental results.

### *Cases*

**Quindici mudflow.** On 4–5 May 1998 more than a hundred slope instabilities occurred on the Pizzo d'Alvano massif, where several mudflows were triggered and travelled down to the towns of Bracigliano, Quindici, Sarno and Siano, located at the toe of the mountain mass. In this section, the major landslide that occurred in San Francesco basin (Quindici sector) is selected and analyzed. The mudflow was triggered by a combination of rainfall infiltration and superficial water fluxes from the bends of the mountain tracks (Revellino *et alii*, 2004). Failure surface was located within the pyroclastic layers, at the top to the particular silty and clayey yellowish basal soil with pumiceousclasts (Revellino *et alii*, 2004), probably attributable to the Campanian Ignimbrite (friction angle between 38 and 45°, residual friction angle more than 25°). The mobilised volume was about 40 000 m$^3$: the length and width of the source area were 250 m and 80 m, respectively; the initial soil thickness was 2 m. Furthermore, the relative water height (i.e. the factor $S$), the consolidation coefficient $c_v$ and the unit weight of involved material (γ) were estimated at 0.25, 1.0·10$^{-2}$ m$^2$/s and 16 kN/m$^3$, respectively (Revellino *et alii*, 2004). The path profile is shown in Fig. 15: the mudflow traveled approximately 1350 m and reached a maximum velocity of 45 m/s.

**Guanling landslide.** On June 28, 2010, a catastrophic landslide occurred in Guanling (Guizhou, China), devasting two villages and killing 99 people. The landslide involved a volume of saturated material (mostly sandstone) of about 985000 m$^3$ and

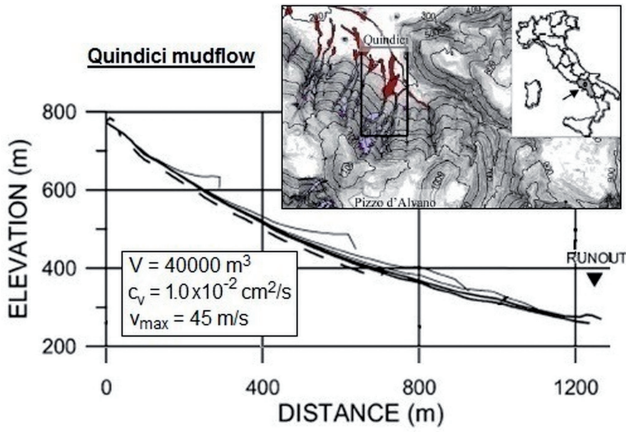


*Fig. 15 - The Quindici mudslide: longitudinal path profile (adapted from* Revellino *et alii, 2004)*

traveled about 1400 m, reaching a maximum speed of 25 m/s, approximately. The altitude profile of the path travelled by the landslide, its thickness (average value = 15 m) and the grain size distribution of the involved material (average grain diameter $d_{50}$ = 0.007 mm) are shown in Fig. 16 (Xing *et alii*, 2015). The basal friction angle (14.4º) was estimated through laboratory tests. The detachment area was characterized by a length of about 400 m and a width of 150-200 m (Xing *et alii*, 2015).

### *Results of numerical simulations*

**Quindici mudflow.** From available data, the following physical and mechanical parameters are selected: $\bar{h}$ = 2 m; $b$ = 250 m (channel width = 80 m); $\gamma$ = 16 kN/m³; $\gamma_{sat}$ = 21 kN/m³; $m_0$ = 7.04·10⁷ kg; $\gamma_{bed}$ = 18 kN/m³; $c_v$ = 0.01 m²/s; $\phi'$ = 27.5°; $S$ = 0.25; $\mu'_e$ = - $\mu'_d$ = 50 kg/m ($m_{fin}$ = 7.4·10⁷ kg, +6 %), 1000 kg/m ($m_{fin}$ = 1.20·10⁸ kg, +72 %).

The *s.s.* has been schematized through an arc of circumference: $\alpha_0$ = 35°; $r$ = 3000 m (geometrical schematization *a*), Fig. 5) (Fig. 17a). The results of simulations are shown in Fig. 17b.

**Guanling landslide.** From available data, the following physical and mechanical parameters are selected: $\bar{h}$ = 15 m; $b$ = 400 m (average channel width = 150 m); $\gamma_{sat}$ = 20 kN/m³; $m_0$ = 1.8·10⁹ kg; $\gamma_{bed}$ = 18 kN/m³; $\phi'$ = 14.4°; $\mu'_e = \mu'_d$ (only erosion) = 1000 kg/m ($m_{fin}$ = 2.05·10⁹ kg, + 14%), 3000 kg/m ($m_{fin}$ = 2.40·10⁹ kg, +33%). The *s.s.* has been schematized through two planes linked by an arc of circumference: $\alpha_1$ = 21°; $\alpha_2$ = 0°, $L_1$ = 650 m, $r$ = 2000 m (geometrical schematization *b*), Fig. 5) (Fig. 18a). The results of simulations are shown in Fig. 18b.

### *Comparison between laboratory and theoretical results*

Laboratory tests were performed with mixtures of water and sediment collected from the Rio Gadria granular flow deposits (Eastern Alps, Italy). The sediment composition of the involved material was characterized by a significative muddy component (Bettella *et alii*, 2015): the average grain diameter ($d_{50}$) and solid concentration ($c_{vol}$) were equal to 1 mm and 0.55, respectively. The experimental apparatus is shown in Fig. 19a: it is composed of flume of length 2 m, width 0.15 m, height 0.40 m, slope angle 20°. During the sliding of the granular mixture, the velocity was measured in four different reference cross sections (Fig. 19 a) of the flume. Information about the values of the consolidation coefficient ($c_v$) and the initial excess pore water pressure ($r_{0,b}$) are not available. To evaluate these coefficients, the following input parameters have been firstly selected: $L_1$ = 2 m; $\alpha_1$ = 20°; $\alpha_2$ = 0° (geometrical schematization *c*) of the s.s., Fig. 5); $\bar{h}$ = 0.20 m; $b$ = 0.15 m; $S$ = 0.5; $\phi$ = 24°; $\gamma$ = 14 kN/m³; $\gamma_{sat}$ = 19 kN/m³; $\mu'$ = 0). By parametrically assigning some values of $r_{0,b}$ and $c_v$, through the proposed solution, the results reported in Figures 19 b, c are obtained.

The best fitting of the kinematics of the considered material flow (curve 1), Fig. 19 d) is obtained if $r_{0,b}$ = *0.90*, falling in the previously defined range (0.85÷0.95) associated with the excess pore water pressure induced by deposition of consolidating

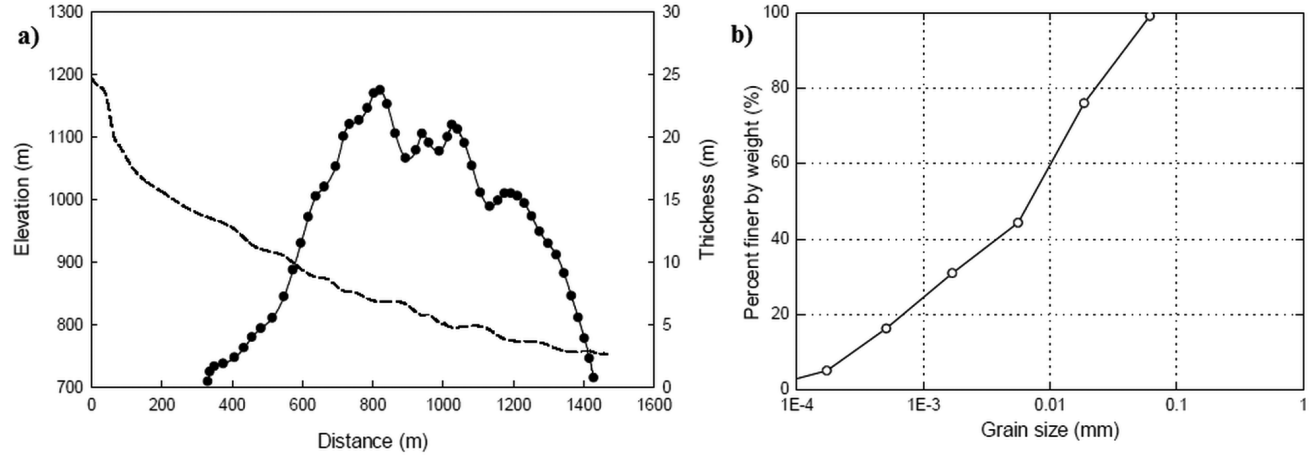


*Fig. 16 - Guanling landslide: a) path profile; b) grain size distribution of the involved materials (*Xing *et alii, 2015)*

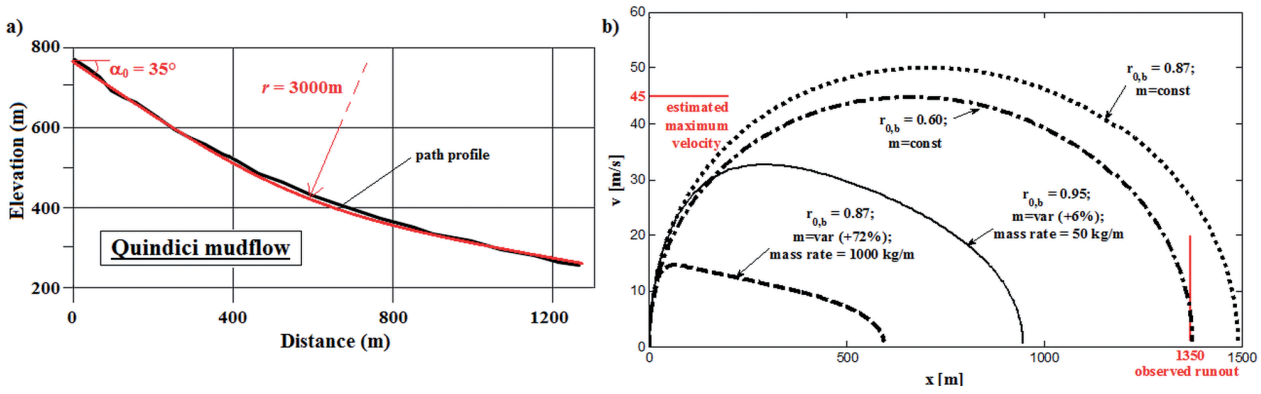


*Fig. 17 - The Quindici mudslide: a) schematization of the sliding surface; b) velocity (v) vs runout distance (x)*

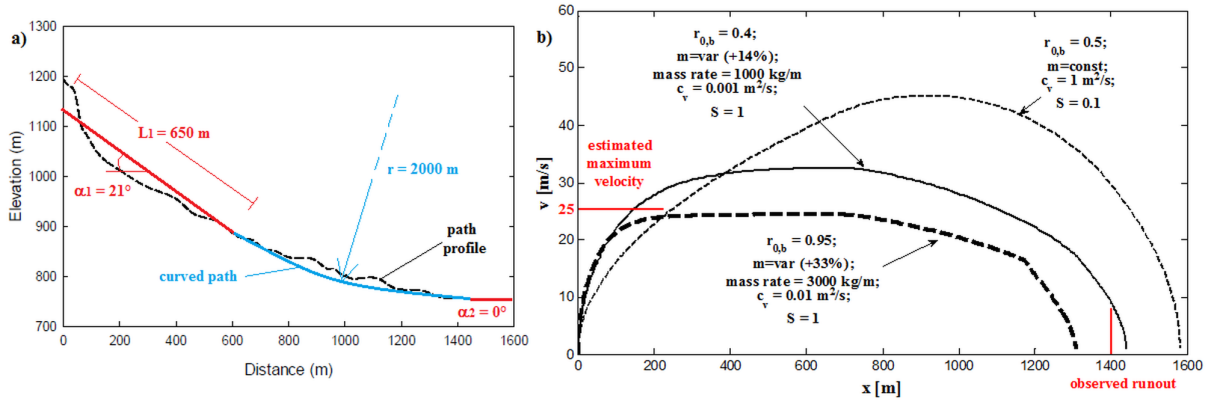


*Fig. 18 - Guanling landslide: a) schematization of the sliding surface; b) velocity (v) vs runout distance (x)*

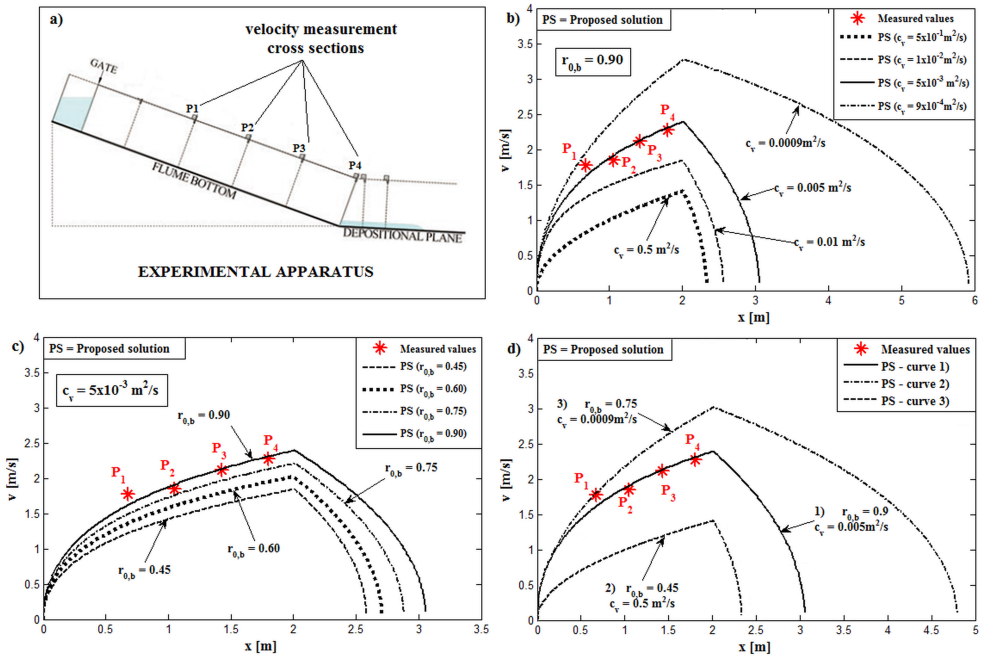


*Fig. 19 - a) Experimental apparatus (adapted from Bettella et alii, 2015). Proposed solution: measured and theoretical velocity (v) vs distance travel (x), for b) several values of $c_v$, fixed $r_{0,b}$; c) several values of $r_{0,b}$, fixed $c_v$. d) Proposed solution: measured and theoretical velocity (v) vs distance travel (x)*

(initially liquefied) mud granular materials, and $c_v$ = *0.005 m²/s*, reasonably corresponding to the tested granular (mud) mixture characterized by an average grain diameter of 1 mm, are selected.

The proposed model takes into account the curvature of the basal surface, only on a vertical plane. Granular flows are often three–dimensional (3D) geotechnical problems and the motion generally occurs along curved, also in the horizontal plane, channels. In order to evaluated the effects of the horizontal curvature of the *s.s.* on the kinematics of granular flows, curved channel tests (Procter, 2012), involving a poorly sorted gravel/sand/clay material ($\gamma^*$ = 18.8 kN/m³, water content = 17% ≡ $S$, $\bar{h}$ = 0.12 m) sliding along a flume 8 m length (at 3.5 m from the headgate, a double horizontal bend is located) are analyzed. Lab measurements show smaller values of velocity at the entrance to the double horizontal bend, respect to the values recorded in straight channel experiments, especially for low values of the curvature radius in the horizontal plane $r_h$. This reduction of velocity suggests that some (energy dissipating) internal processes (e.g. compression of material due to centrifugal force at the outer side of the bend) occur within the mass flowing along the curved channel (Daniels & Rhoads, 2004; Procter, 2012). It is interesting to observe that a similar reduction of flow velocity along curved (on the vertical plane) channels can be obtained through the proposed model; to this purpose, the following geometry of the sliding surface (Fig. 20): $L_1$ = 3.5 m, $r$ (curvature radius in the vertical plane) = $r_h$ (curvature radius in the horizontal plane) = 0.40 and 0.70 m; $\alpha_1$ = 23° and 25°, $\alpha_2$ = $\alpha_h$ - $\alpha_1$ ($\alpha_h$ = bend angle) is considered. By neglecting the mass variation ($\mu'$=*0*), the consolidation process, $u_{b0}$ (= 0) and $\Delta p_{w,b,\Delta N}$ (= 0), the results shown in Fig. 20 are obtained: the reduction in velocity along the curved path obtained through the proposed model (curvature on the vertical plane) by replacing the horizontal curvature with the vertical one is close to that one measured in laboratory (curvature on the horizontal plane).

Thus, the effects of the horizontal curvature on the motion are similar to those due to the vertical one and cannot be neglected. Definitively, the curvature (on the vertical and horizontal planes) of channels can induce significant effects on the motion due to changes of stress state ($\Delta N$), excess pore water pressure ($\Delta p_w$) and flow velocity, which in turn greatly influence the sliding of granular flows.

## *Observations*

A reasonable interpretation of observed values of runout distance and maximum velocity is obtained by assuming: 1) for Quindici mudflow, $\mu'$ = 0 (constant mass) and $r_{0,b}$ = 0.6 (Fig. 17 b); 2) for Guanling landslide, $\mu' \neq 0$ (variable mass); $S$ = 1 ( saturated flow) and values of $c_v$ (0.01 m²/s) reasonably corresponding to the involved materials, characterized by an average grain diameter of 0.007 mm (Fig. 18 b).

Thus, the results reported in Figs. 17, 18 show the role played by the parameters previously introduced, i.e. the mass variation, the slope curvature, the evolution of excess pore water pressures, necessary for a reliable interpretation of considered cases.

To better understand the role of the increments of pore water pressure due to curvature coupled to undrained conditions on the kinematics of fine-grained material flows, the following parameters are considered: $\alpha_1$ = 20-25-30°; $L_1$ = 100-500-1000 m; $\alpha_2$ = 0°; $r$ = 500-1000-2000-3000 m (geometrical schematization *b*) of the *s.s.* Fig. 5); $\phi'$ = 20-25°; $\bar{h}$ = 5 m; $S$ = 1; $u_{b,0}$ = *0* (no initial excess pore water pressure and successive dissipation); $\gamma$ = 14 kN/m³; $\gamma_{sat}$ = 19 kN/m³; $\mu'_e$ = $\mu'_d$ = 0 (constant mass). If $H_g$ (geodetic elevation referred to the mass center of the block) is defined as $L_1 \cdot \sin(\alpha_1)$, then, for $\alpha_1$ = 25° and $L_1$ = 100 m, $H_g$ = 42 m; for $\alpha_1$ = 20° and $L_1$ = 500 m, $H_g$ = 171 m; for $\alpha_1$ = 30° and $L_1$ = 1000 m, $H_g$ = 500 m. The results, in terms of total runout distance, according to the cases shown in Table 2, are reported in Fig. 21.

An appreciable difference between the computed values of

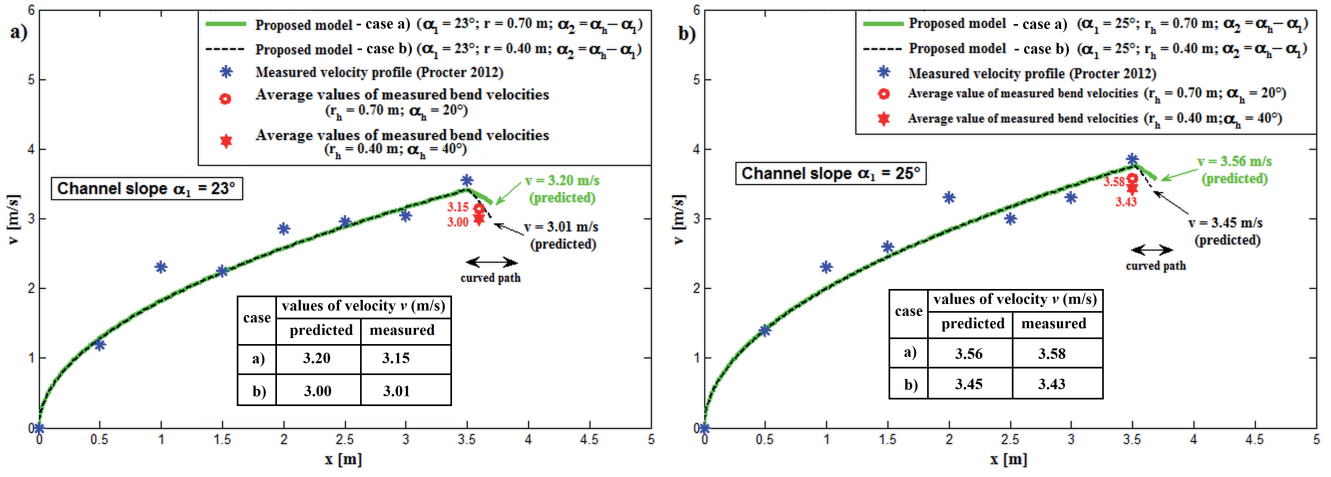


*Fig. 20 - tests results vs proposed solutions: velocity (v) vs travelled distance (x) for a) $\alpha_1$ = 23°; b) $\alpha_1$ = 25°.*

runout length in the analyzed cases is observed, expecially for high values of $H_g$ (Fig. 21b) and smaller values of ϕ' (Fig. 21 a), causing higher values of the sliding rate. Higher values of the runout length are obtained in the case *D* (simulataneously presence of $\Delta p_{w,b,k}$; $\Delta p_{w,b,\Delta N}$).

## CONCLUDING REMARKS

Rheological laws for fluid and granular flows available in literature are firstly discussed through the analysis of the typical mechanical behaviour of normal stream flows, hyperconcetrated flows, mudflows, debris flows, rock avalanches and their multiphase nature (flow like or granular). Afterwords, the rapid sliding of fine – grained material flows, taking into account the curvature of the basal surface (on a vertical plane), the variation of its mass due to erosion processes as well as the evolution of pore water pressures, is modelled.

To estimate the distance traveled by the material, an analytical ("block") model is proposed. The dissipation of the initial basal excess pore water pressures (these last ones induced by cyclic loads or deposition of liquefied mud masses), due to consolidation process, as well as the pore water pressure increments associated with coupled slope curvature and undrained conditions, are taken into account.

The differential equation, describing the sliding of the block, has been numerically integrated. To evaluated the role of the considered additional factors (e.g. slope curvature, mass variation, sudden pore water pressure increase), several parametrical analyses have been carried out. Results show that for high $c_v$ values (coarse sand), the approximate condition $u_b = 0$ can be assumed; for small *cv* values (silt and clay) the approximate condition $ub = u_{b0} = constant$ can be imposed. It has been demonstrated that even a small increase in the sliding mass due to erosion phenomena induces appreciable reductions of travelled distance and maximum velocity.

It is worth observing that, although the excess pore water pressure may vanish at the end of the curved path, the sliding mass may exhibit remarkable increases in its velocity, particularly in case of high values of the curvature radius.

These aspects, coupled with opposite effects associated with consolidation, are neglected in conventional empirical relationships and in available models.

The significance of the effects of these peculiarities is underlined by the review of documented cases (Quindici mudflow and Guanling landslide) and laboratory measurements. The relevant analyses validated the proposed model and showed that the introduced additional features allow a better interpretation and modeling of the rapid sliding phenomena under examination. The effects associated with curved (also in the horizontal plane) flow channels are also discussed.

The main limits of the proposed model lie in the simplified geometry of the sliding mass body (parallelepipedal shape) and of the sliding surface (curvature of the basal surface only

| CASE | $\Delta p_{w,b,k}$ | $\Delta p_{w,b,\Delta N}$ |
|---|---|---|
| A (effects related to curvature and to undrained conditions are neglected) | = 0 | = 0 |
| B (effects related to undrained conditions are neglected) | ≠ 0 | = 0 |
| C (the coupled effects related to curvature and undrained conditions are only considered) | = 0 | ≠ 0 |
| D (coupled effects related to curvature and to undrained conditions are considered) | ≠ 0 | ≠ 0 |

*Tab. 2 - Evaluation of the effects of the increments of pore water pressure: analyzed cases*

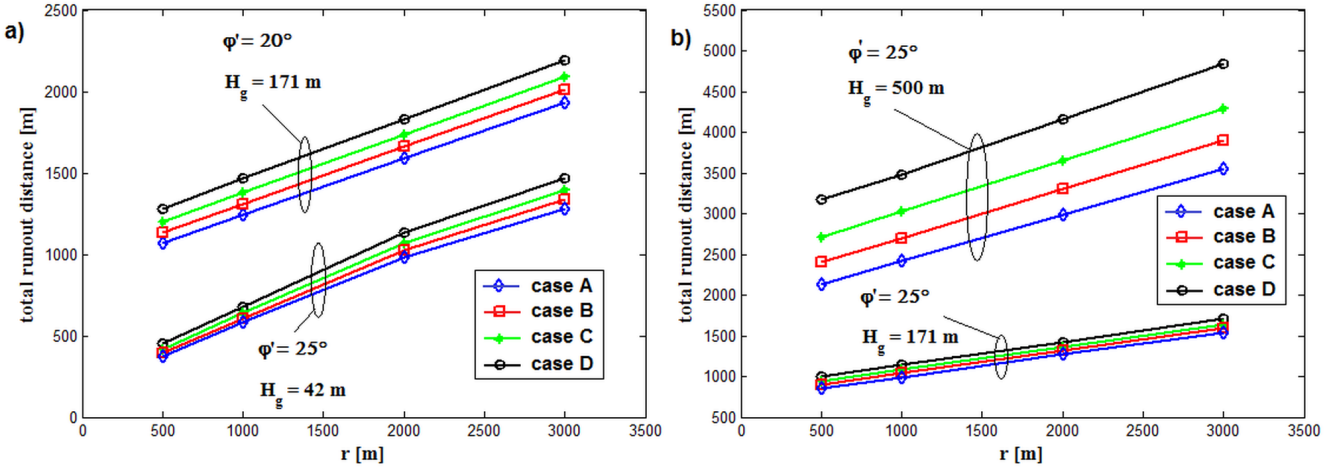


*Fig. 21 - Total runout length vs curvature radius (r) in absence or presence of the increments of pore water pressure $\Delta p_{w,b,k}$,$\Delta p_{w,b,\Delta N}$, for a) $H_g$ = 42 m and 171 m, ϕ' = 20° and 25°; b) $H_g$ = 171 m and 500 m, ϕ' = 25°*

in the vertical plane), in the assignment of the law $u_b(t)$, in the assumptions of 1-D consolidation process and of linear-elastic behaviour of the involved material.

## NOTATION

$a$ = empirical coefficient related to consolidation process
$a_i$ = Bagnold constant
$A$ = coefficientin the expression to estimate $r_{b,0}$
$b$ = flow length
$B$ = coefficientin the expression to estimate $r_{b,0}$
$c_v$ = consolidation coefficient ($m^2/s$)
$c_{vol}$ = volume concentration
$c_{max}$ = maximum volume concentration
$C_{pw}$ = pore water pressure parameter for loading processes under edometric and undrained conditions
$d_p$ = representative grain diameter
$d_{50}$ = average grain diameter corresponding to 50% weight passing
$E_{ed}$ = oedometric modulus
$f_1$, $f_2$, $f_3$ = coefficients in the compact form of eq. (30)
$F$ = resultant of forces acting on the block
$g$ = gravity acceleration
$\overline{h}$ = flow depth
$H$ = maximum drainage distance
$H_g$ = geodetic elevation
$k$ = permeability coefficient
$l_m$ = mixing length by Prandtl
$L_1$ = length of the first slope
$m$ = mass of the block
$m_0$ = initial mass of the block
$m_{fin}$ = final mass of the block
$\dot{m}$ = mass variation rate
$N$ = resultant of the total vertical stresses at the base
$N_{Ba}$ = Bagnold number
$OCR$ = over consolidation ratio
$p_w$ = pore water pressure
$p_{w,t0}$ = initial pore water pressure at the top of the saturated layer
$p_{w,b0}$ = initial pore water pressure at the base of the saturated layer
$p_{w,b}$ = basal pore water pressure
$p_{w,hyd}$ = hydrostatic interstitial pressure
$p_{w,b,hyd}$ = basal hydrostatic interstitial pressure
$PI$ = plasticity index
$\widehat{PR}$, $\widehat{PQ}$ = curved paths in Fig. 9a
$r$ = curvature radius (on the vertical plane)
$r_h$ = centreline curvature radius (on the horizontal plane)
$r_b$ = curvature radius at the base of the sliding block
$r_1$, $r_2$ = curvature radius on Fig. 9a
$r_{0,b}$ = ratio between the current initial basal excess pore water pressure and its maximum value
$r_s$ = splitting function
$\overline{r}_s$ = complementary splitting function
$s$ = curvilinear abscissa
$\dot{s}$ = velocity of the granular flow along the curved path
$\ddot{s}$ = acceleration of the granular flow along the curved path
$s_0$ = origin of the curvilinear abscissa
$S$ = percentage of saturated layer $\epsilon$ [0,1]
$t$ = time instant
$t_0$ = initial instant
$\overline{t}$ = instant at which the mass begins to slide along the second slope
$T_{max}$ =shear resistance force
$u$ = excess pore water pressure
$u_b$ = basal excess pore water pressure
$u_{t0}$ = initial excess pore water pressure at the top of the saturated layer
$u_{b0}$ = initial basal excess pore water pressure
$u_{b0,max}$ = maximum initial basal excess pore water pressure
$U$ = pore water pressure resultant
$v$ = flow velocity
$v_0$ = initial flow velocity
$w^*$ = velocity of the incorporated or lost mass
$x$ = distance traveled by the center of mass of the block
$x_{max}$ = maximum traveled distance
$\dot{x}$ = velocity of the granular mass
$\ddot{x}$ = acceleration of the granular mass
$x_0$ = initial distance traveled by the center of mass of the block
$x_e$ = abscissa at which the erosion/deposition processes begin to occur
$\overline{z}$ = coordinate perpendicular to the plane (x ,y) along which the motion occurs
$\alpha$ = angle of slope of the sliding surface
$\alpha_0$ =slope of the sliding surface at the beginning of the curved path and/or the motion
$\alpha_1$ =first slope
$\alpha_2$ = second slope or counterslope
$\alpha_h$ = bend angle
$\beta_e$ = erosion critical slope
$\gamma$ = unit weight of the involved material
$\gamma_{bed}$ = unit weight of the material lying on the channel bed
$\gamma_w$ = water unit weight
$\gamma_{sat}$ = unit weight of the saturated material
$\gamma_s$ = soil unit weight
$\gamma^*$ = unit weight of the flow
$\gamma'$ = submerged soil unit weight
$\gamma_{c,max}$ = maximum shear strain
$\gamma_{av}$ = average shear strain
$\Delta p_{w,b}$ = additional basal pore water pressure
$\Delta p_{w,\Delta N}$ = additional pore water pressure due to increase of the total normal stresses along the curved path
$\Delta p_{w,b,\Delta N}$ = additional basal pore water pressure due to increase of the total normal stresses along the curved path
$\Delta p_{w,k}$ = additional pore water pressure due to slope curvature of the sliding surface

$\Delta p_{w,b,k}$ = additional basal pore water pressure due to slope curvature of the sliding surface
$\Delta\sigma_{\Delta N}$ = increment of total normal stresses
$\Delta\sigma_{b,\Delta N}$ = increment of basal total normal stresses
$\Delta t$ = integration time interval
$\Delta u$ = excess pore water pressure
$\Delta v$ = velocity variation along the curved path
$\Delta x$ = curved path length
$\eta$ = experimental coefficient in the expression to estimate $r_{b,0}$
$\lambda$ = linear concentration
$\mu_b$ = Bingham viscosity
$\mu_f$ = dynamic viscosity of interstitial fluid
$\mu_c$ = dispersive parameter
$\mu_t$ = turbulent parameter
$\mu'$ = erosion/deposition rate
$\mu'_e$ = erosion rate
$\mu'_d$ = deposition rate
$\sigma$ = total stress
$\sigma'$ = effective stress
$\tau_c$ = cohesion
$\tau_{mc}$ = frictional shear stress
$\tau_y$ = shear stress according to Mohr-Coulomb resistance law ($\tau_c + \tau_{mc}$)
$\tau_v$ = shear stress according to Bingham model
$\tau_t$ = turbulent shear stress
$\tau_d$ = dispersive shear stress
$\tau_{fr} = \tau_y$
$\tau_{disp} = \tau_d$
$\tau_{max}$ = resistance shear stress
$\phi'$ = friction angle along the sliding surface
$\Psi$ = ratio between the excess pore water pressure due to slope curvature and the basal hydrostatic pressure
$\Omega$ = basal area of the sliding block

## REFERENCES


Armanini A., Fraccarollo L. & Larcher M. (2003) - *Dynamics and energy balances in uniform liquid-granular flows.* International Workshop on Occurrence and Mechanisms of Flows in Natural Slopes and Earthfills IW-Flows, Sorrento, Pàtron Editore, 131-138.

Armanini A., Fraccarollo L. & Larcher M. (2008) - *Liquid-granular channel flow dynamics*. Powder Technology, **182** (2): 218-227. Doi: 10.1016/j.powtec-2007.08.012.

Armanini A. (2010) - *La modellazione idraulica dei fluidi bifasici solido liquido*. Atti del XXXII Convegno Nazionale di Idraulica e Costruzioni Idrauliche, Palermo, Walter Farina Editore, 133-161.

Armanini A. (2013) - *Granular flows driven by gravity.* Journal of Hydraulic Research, **51** (2): 111-120. Doi: 10.1080/00221686.2013.788080.

Bagnold R.A. (1954) - *Experiments on a gravity-free dispersion of large solid spheres in a Newtonian fluid under shear*. Roy. Soc. London 225: 49-63.

Bettella F., Bischetti G.B., D'Agostino V., Marai S.V., Ferrari E. & Michelini T. (2015) - *Comparison of measurement methods of the front velocity of small scale debris flows*. J. of Agricultural Engineering, **46** (4).

Cannon S.H. & Savage W.Z. (1988) - *A mass-change model for the estimation of debris-flow runout.* Journal of Geology, **96**: 221-227.

Charles W.W.N.G. (2014) - *The state of the art centrifuge modelling of geotechnical problems at HKUST*. Journal of Zhejiang University – Science A (ApplPhys&Eng), **15** (1): 1-21.

Chian S.C. (2015) - *Empirical excess pore pressure dissipation model for liquefiable sands*. Proc. 6th International Conference on Earthquake Geotechnical Engineering, Christchurch, New Zealand.

Ciabatti M. (1964) - *La dinamica della frana del Vajont*. Giornale di Geologia, **32** (1): 139-160.

Comegna L. & Picarelli L. (2005) - *The interplay between pore pressures and slope movements in fine-grained materials*. Proc. 11th IACMAG, Turin.

Costa J.E. (1984) - *Physical geomorphology of debris flow.* Springer-Verlag Berlin Heidelberg.

Coussot P. & Meunier M. (1996) - *Recognition, classification and mechanical description of debris flows*. Earth Science Reviews, **40**: 209-227.

Crosta G.B. & Dal Negro P. (2002) - *Observations and modelling of soil slip-debris flow initiation processes in pyroclatic deposits: the Sarno 1998 event.* Natural Hazards and Earth System Sciences, **3**: 53-69.

Daniels D.M. & Rhoads B.L. (2004) - *Effect of large woody debris configuration on three-dimensional flow structure in two low-energy meander bends at varying stages.* Water Resources Research, **40**: W11302, Doi:10.1029/2004WR003181.

Davies T.R.H. (1988) - *Debris flow surges - a laboratory investigation*. Mitteilungen der Versuchsanstalt für Wasserbau, Hydrologie und Glaziologie, Nr. 96, ETH Zürich, Switzerland.

De Marchi G. (1961) - *Idraulica. Basi scientifiche e applicazioni tecniche*. Ulrico Hoepli, Milano.

Federico F. & Cesali C. (2015) - *An energy-based approach to predict debris flow mobility and analyze empirical relationships*. Canadian Geotechnical Journal, **52** (12): 2113–2133. Doi:10.1139/cgj-2015-0107.

Federico F. & Cesali C. (2016) - *Flussi detritici ad alta velocità. Modellazione e simulazioni numeriche*. L'Acqua n. 1-2/2016: 37-65.

Federico F. & Cesali C. (2016) - *Flussi detritici ad alta velocità. Modellazione e analisi critica di criteri empirici.* L'Acqua n. 3/2016: 5-38.

Federico F. & Cesali C. (2017) - *Coupled effects of pore water pressures evolution, slope curvature and mass variation on the kinematics of rapidly sliding fine-grained materials*". International Journal of Geomechanics (ASCE), in press.

Fernández-Merodo J.A., Herrera G., Mira P., Mulas J., Pastor M., Noferini L., Mecatti D. & Luzi G. (2008) - *Modelling the Portalet landslide mobility (Formigal, Spain)*. Proc. International Environmental Modelling and Software Society (iEMSs), 1476-1483.

Fukuoka H. (1991) - *Variation of the friction angle of granular materials in the high-speed high-stress ring shear apparatus influence of re-orientation, alignment and crushing of grains during shear.* Bulletin of the Disaster Prevention Research Institute, **41** (4): 243-279.

Huang M.C. (2003) - *The numerical simulation of the range of debris-flow hazards and detection of debris-flow by using microwave.* Ph.D Dissertation, Department of Civil engineering, National Taiwan University.

Hungr O. (1995) - *Model for the runout analysis of rapid flow slides, debris flows, and avalanches*. Can. Geotech. Journal, **32**: 610-623.

Hungr O. & Evans S.G. (1996) - *Rock avalanche run out prediction using a dynamic model*. Proceeding 7th International Symposium on Landslides, 1, 233-238, Trondheim, Norway.

Hungr O. (2004) - *Flow slides and flows in granular soils*. Proc. Int. Workshop on Occurrence and Mechanisms of Flow-Like Landslidesin Natural Slopes and Earthfills, Sorrento, Picarelli ed., Kluwer Publishers.

Hungr O. & Morgenstern N.R. (1984) - *High velocity ring shear tests on sand*". Geotechnique, **34**: 415-421.

Hutchinson J.N. (1986) - *A sliding consolidation model for flow slides*. Can. Geotech. J., **23**: 115-126.

Hutchinson J.N. & Bhandari R.K. (1971) - *Undrained loading, a fundamental mechanism of mudflows and other mass movements.* Geotechnique, **21**: 353–358.

Ikeya H. (1981) - *A method of designation for area in danger of debris flow. Erosion and sediment transport in Pacific Rim, Steeplands*. I.A.H.S.,Publ. No. 132, Christchurch, 576-588.

Iverson R.M. (1997) - *The physics of debris flows*. American Geophysical Union.

Iverson R.M., Reid M.E. & LaHusen R.G. (1997) - Debris-flow mobilizationfrom landslides. Proc.,Annu. Rev. Earth Planet. Sci., **25**: 85-138.

Julien P.Y. & Lan Y. (1991) - *Rheology of hyperconcentrations*. J. of Hydr. Engineering, **117** (3): 346-353.

Julien P.Y. & Paris A. (2010) - *Mean velocity of mudflows and debris flows*. J. of Hydraulic Engineering, **136**: 676–679.

Lambe T.W. & Whitman R.V. (1969) - Soil Mechanics. John Wiley and Sons, 553 pp.

Liu K.F. & Huang M.C. (2006) - *Numerical simulation of debris flow with application on hazard area mapping.* Computational Geoscience, **10** (2): 221-240.

Lollino P., Giordan D. & Allasia P. (2014) - *The Montaguto earthflow: a back analysis of the process of landslide propagation.* Engineering Geology, **170**: 66-79.

Macedonio G. & Pareschi M.T. (1992) - *Numerical simulation of some lahars from Mount St Helens*. J. of Volcanology and Geothermal Research, **54**: 65-80.

Miao T., Liu Z., Niu Y. & Ma C. (2001) - *A sliding block model for the runout prediction of high speed landslides*. Canadian Geotechnical J., **38**: 217-226, Doi: 10.1139/cgj-38-2-217.

Miao H., Wang G., Yin K., Kamai T. & Li Y. (2014) - *Mechanism of the slow-moving landslides in Jurassic red-strata in the Three Gorges Reservoir, China*. Engineering Geology, **171**: 59-69.

Nemec W. (2009) - *What is a hyperconcentrated flow?* Annual Meeting of the International Association of Sedimentologists, Alghero (Sardinia), 20–23 September 2009.

Novosad J. (1964) - *Studies on granular materials. Apparatus for measuring the dynamic angle of internal and external friction of granular materials.* Collection Czech. Chem. Commun., **29**: 2697-2701.

O'Brien J.S. & Julien P.Y. (1985) - *Physical properties and mechanics of hyperconcentrated sediment flows.* Proc. Specialty Conf. on Delineation of Landslides, Flash Flood and Debris Flow Hazards in Utah, Utah Water Research Laboratory, Utah State Univ., Logan, Utah, 260–279.

O'Brien J.S. & Julien P.Y. (1988) - *Laboratory analysis of mudflow properties*. Journal of Hydraulic Engineering, **110**: 877-887.

Park D., Lee S., Nikhil N.V., Kang S. & Park J. (2013) - *Debris flow hazard zonation by probabilistic analysis*. International Journal of Innovative Research in Science, Engineering and Technology, **2** (6): 2381-2390.

Pellegrino A., Picarelli L. & Urciuoli G. (2004) - *Experiences of mudslides in Italy*. Proc. Int. Workshop on Occurrence and Mechanisms of Flow-Like Landslidesin Natural Slopes and Earthfills, Sorrento, Picarelli Ed., 191-206.

Peng S.H. & Lu S.C. (2012) - *FLO-2D simulation of mudflow caused by large landslide due to extremely heavy rainfall in Southeastern Taiwan during Typhoon Morakot*. J. Mt. Sci., **10** (2): 207-218. Doi: 10.1007/s11629-013-2510-2.

Picarelli L. (1988) - *Modellazione e monitoraggio diuna colata in formazioni strutturalmente complesse*. Proc., Conf. on Problemi di Cartografia e di Monitoraggio dei Fenomeni Franosi, Bologna, Cascini ed., 2, 119-130.

Picarelli L. & Russo, C. (2004) - *Remarks on the mechanicsof slow active landslides and the interactionwith man-made works.* In. Lacerda W.A., Erlich M., Fontoura S.A.B. & Sayão A.S.F. (Eds.). Proc. 9th Int. Symp. on Landslides, Rio de Janeiro, Balkema, Rotterdam, 2, 1141-1176.

Pierson T.C. & Costa J.E. (1987) - *A rheologic classification of subareal sediment flows*. Reviews in Engineering Geology, VII Debris flow/Avalanches: process, recognition and mitigation, Costa J.E. & Wieczoreck Eds, Geolocical Society of America, Boulder, Colorado 7, 1-12.

Procter C.M. (2012) - *Debris flow dynamics: a flume study of velocity and superelevation*. Durham theses, Durham Univ.

Revellino P., Hungr O., Guadagno F.M. & Evans S.G. (2004) - *Velocity and runout simulation of destructive debris flows and debris avalanches in pyroclastic deposits, Campania region, Italy*. Environmental Geology, **45**: 295–311.

Scarllett B. & Todd A.C. (1968) - *The critical porosity of free-flowing solids.* J. Engng. Ind. Ser. A, **91**: 478-488.

Siviglia A. & Cantelli A. (2005) - *Effect of bottom curvature on mudflow dynamics: theory and experiments.* Water Resources Research, **41**: 1-17.

Skempton A.W. (1985) - *Residual strength of clays in landslides, folded strata and the laboratory*. Geotechnique, **35**: 3-18.

Smith G.A. (1986) - *Coarse-grained nonmarinevolcaniclastic sediment: terminology and depositional process*. Bull. Geol. Soc. Am., **97**: 1-10.

Takahashi T. (1991) - *Debris flow.* IAHR Monograph Series, Rotterdam, Balkema Publishers.

Take W.A. & Beddoe R.A. (2014) - *Base liquefaction: a mechanism for shear-induced failure of loose granular slopes.* Can. Geotech. J., **51**: 496-507.

Tika T.E. & Hutchinson J.N. (1999) - *Ring shear tests on soilfrom the Vajont landslide slip surface.* Geotechnique, **49**: 59-74.

Van Grassen W. & Cruden D.M. (1990) - *Momentum transfer in the debris of rock avalanches*. Canadian Geotechnical Journal, **27**: 623-628.

Varnes D.J. (1978) - *Slope movement types and processes.* In: Schuster R.L & Krizek R.J. (Eds.). Special Report 176: Landslides: Analysis and control, Transportation and Road research board, National Academy of Science, Washington D.C. 11-33.

Wang G., Suemine A. & Schulz W.H. (2010) - *Shear-rate-dependent strength control on the dynamics of rainfall-triggered landslides, Tokushima Prefecture, Japan*. Earth Surface Processes and Landforms, **35** 407-416.

Widjaja B., Setiabudi D.W. & Arista I. (2014) - *Reccomendation of viscosity values of mudflows*. Int. Conf. on Env. Friend. Civil Eng. Construction and Materials, Manado, Indonesia, November 2014: 401-405.

Xing A., Wang G., Li B., Jiang Y., Feng Z. & Kamai T. (2015) - *Long-runout mechanism and landsliding behaviour of a large catastrophic landslide triggered by a heavy rainfall in Guanling, Guizhou, China.* Canadian Geotechnical Journal, **52** (7): 971-981, Doi: 10.1139/cgj-2014-0122.

Zic E., Arbanas Z., Bicanic N. & Ozanic N. (2015) - *A model of mudflow propagation downstream from the Grohovo landslide near the city of Rijeka (Croatia).* Nat. Hazards Earth Syst. Sc., **15**: 293-313. Doi:10.5194/nhess-15-293-2015.

*Received December 2016 - Accepted May 2016*